ANALYSIS OF PULSE DETONATION TURBOJET ENGINES

by

RONNACHAI VUTTHIVITHAYARAK

Presented to the Faculty of the Graduate School of

The University of Texas at Arlington in Partial Fulfillment

of the Requirements

for the Degree of

DOCTOR OF PHILOSOPHY

THE UNIVERSITY OF TEXAS AT ARLINGTON

December 2011

ACKNOWLEDGEMENTS

I would like to express my most sincere gratitude towards my advisor Dr. Frank K. Lu for constantly motivating and encouraging me, and also for his invaluable advice during my doctoral studies. I would also like to thank the other members of my committee, Dr. Don Wilson, Dr. Luca Massa, Dr. Luca Maddalena, and Dr. Cheng Luo for their interest and for their valuable time and advice on this research.

Also, I would like to extend my appreciation to the Royal Thai Air Force for providing financial support and opportunity for my doctoral studies. I wish to thank all the members of the Aerodynamic Research Center (ARC) for their support and encouragement, especially Eric M. Braun for his help on the Cantera coding and the Endo–Fujiwara modeling. Further, various elements of this study are based on a number of previous research studies at the ARC. I wish to acknowledge the persons involved with the earlier work.

Finally, special acknowledgement goes to my family for their sacrifice, encouragement and patience. Without them, graduate school in the United States would have been impossible. I also thank my friends who have helped me throughout my studies. Further, I am grateful to all the teachers who taught me during the years I spent in school, in both Thailand and the United States.

August 25, 2011

ABSTRACT

ANALYSIS OF PULSE DETONATION TURBOJET ENGINES

RONNACHAI VUTTHIVITHAYARAK, Ph.D.

The University of Texas at Arlington, 2011

Supervising Professor: Frank K. Lu

Research over the last two decades has shown the potential advantages of pulse detonation engines (PDEs) over existing aero-engines in terms of improved thermodynamics efficiency, improved thrust performance, simplicity of design, and flexibility to operate over a wide speed range. The inherently unsteady characteristic of PDEs makes it difficulty to analyze and evaluate their performance. The conventional method that relies on steady-state assumptions cannot be directly applied. PDE studies have to employ unsteady gasdynamics behavior. In this study, the thermodynamic cycle of a PDE, which can be called the ZND cycle, is theoretically analyzed. A parametric analysis of turbojet PDEs is considered for both ideal and non-ideal cases. The conventional turbojet with a Brayton cycle is brought in the comparison to verify that PDEs can provide better performance.

TABLE OF CONTENTS

LIST OF ILLUSTRATIONS

LIST OF TABLES

CHAPTER 1

INTRODUCTION

1.1 Introduction

Airbreathing pulse detonation engines (PDEs) are considered to yield better performance than existing aero-engines in terms of improved thermodynamic efficiency, simplicity of manufacture and operation and high thrust-to-weight ratio, amongst others. Much effort has been put into the development of PDEs over the past two decades, from fundamental detonation studies aimed specifically toward hardware development, to hardware development itself, as well as numerical modeling and cycle analysis. Thermodynamic analysis of PDEs usually makes use of one-dimensional models, based on the Chapman–Jouguet (CJ) and the Zel'dovich–von Neumann–Döring (ZND) theories, although increasingly sophisticated techniques partly involving numerical modeling have also been developed lately. Early work on detonation cycles approximated the detonation process by a constant volume one. This is generally called the *Humphrey* cycle after its first proponent [1]. It is now understood that the Humphrey cycle underpredicts the performance of a PDE [2, 3, 4] The so-called *Fickett–Jacobs* cycle relies on the CJ theory for the detonation process. While an improvement over the Humphrey cycle, its reliance on the CJ model means that it fails to account for the physics espoused by the ZND model [5, 6].

The detonation process in the ZND model can be considered to consist of a shock along an inert Hugoniot to achieve the compressed ZND state that triggers chemical reactions. Heat release from the chemical reactions then results in the gas attaining the CJ state. Subsequently, depending on the upstream boundary

conditions, the gas generally undergoes an isentropic expansion, known as the Taylor expansion. The theoretical cycle closes when the gas returns to its initial state. Experimental observations indicate that the detonation front is actually a complex, three-dimensional surface that defies any simplified analytical description. Thus, despite the one-dimensional nature of the ZND model, it is presently acceptable for engineering analysis. We call this the *Zel'dovich–von Neumann–Döring* cycle.

Standard thermodynamic cycle analysis has been performed on PDEs to understand their performance, some of these studies of which were cited above. Some studies have attempted to compare the detonation engine, whether modeled by the Humphrey, FJ or ZND models, against a conventional, turbomachinery jet engine based on the Brayton cycle. While the jet engine is regarded to be a continuous device, a detonation engine is intermittent, analogous to the internal combustion, reciprocating engine. Briefly, the processes in a PDE are filling of the detonation tube with propellant, initiating the detonation, propagating the detonation wave, and exhausting the burned products. Adequate understanding of the way PDEs operate has allowed cycle analysis to be applied effectively.

1.2 Literature Review

1.2.1 Historical Review

There have been efforts to utilize the energy release obtained from explosions for propulsion since the late 17th to early 18th centuries. For instance, Clerk [7] mentioned that Huyghens proposed using gunpowder for motive power in 1680. Clerk also discusses the constant volume engine, developed later by Humphrey [1] amongst others. Allen [8] mentioned a jet propeller ship which operated from the explosion of gun powder in 1729. In fact, the late 19th and early 20th centuries were rife with

proposals to harness explosions for work. Instead of gunpowder, gas explosions were first independently recognized by Berthelot [9, 10], and Mallard and Le Chatelier [11] in the early 1880s. These investigators discovered a combustion mode that arose when an explosive gaseous mixture was ignited by a non-explosive means in a long tube. They proposed that a detonation propagates as an adiabatic compression wave. Further, they indicated that the detected detonation velocity was primarily a function of the explosive mixture composition and does not depend on the ignition source and tube diameter. The studies relied on O_2 mixtures of H_2, CH_4, C_2H_2, C_2H_6, C_2N_2 in tubes.

In 1899, Chapman [12] stated that the minimum speed with respect to the burned gas is equal to the speed of sound in the gas. His conclusion is based on the shock wave theory of Rankine [13] and Hugoniot [14, 15] which were proposed in 1870 and 1887 respectively [16]. In 1899, Vieille [17, 18] reported the use of a shock tube that compared the shock wave speed with Hugoniot's theory. A few years later, Jouguet [19] applied Hugoniot's method to derive the detonation velocity. He illustrated that the main properties of a detonation wave propagating at constant velocity can be described by assuming that, behind the wave front, the velocity of the reactants with respect to the detonation wave front is equal to the local sound velocity. The classic Chapman–Jouguet (CJ) theory was established from these proposals. This theory demonstrated that the CJ velocity can be evaluated by mean values of specific heat capacity that were based on extrapolating low temperature experimental data. In 1910, Taylor computed the structure of a weak wave from the Navier–Stokes equations and the conservation of energy with a thin layer where entropy is generated; see [20].

The discovery of spinning detonation by Campbell and Woodhead [21] in 1926 recognized that detonation waves are more complex than expression of Chapman–

Jouguet theory. Photographs of detonation mixtures depicted an undulating front with striations behind it, with hot and luminous regions rotating around the axis of the tube as the detonation advances. Campbell and Woodhead's discovery led to numerous studies of the detonation wave structure. During the same period, Payman [22, 23, 24] observed deflagration-to-detonation transition (DDT) using high-speed photography. These studies revealed that the igniter spark does not affect the pressure waves in front of the flame. The waves propagate at a velocity that is greater than velocity of sound and appear to have their origin in the gases behind the flame front.

In 1940, Zel'dovich [25] developed a theory of detonation wave structure and detonation ability limit. He proposed a model of one-dimensional structure of a detonation wave comprising of a lead shock wave, which provides adiabatic compression and heating of the fresh explosive mixture, followed by reaction front taking into account the finite-rate chemistry. A few years later, von Neumann [26] and Döring [27] independently formulated similar models as Zel'dovich. At present, these are collectively recognized as the Zel'dovich–von Neumann–Döring (ZND) model. The basic ZND model consists of a shock wave that compresses gas from the initial state along the inert Hugoniot to achieve a high enthalpy state known as the von Neumann spike. The subsequent chemical reactions heat the gas along a Rayleigh line process to the CJ point. This ZND model is physically well-based and is a helpful idealization of a real detonation wave, it was obviously illustrated both experimentally and theoretically that a detonation is essentially three-dimensional and steady-state only on average. Furthermore, this realistic three-dimensional structure raised complications concerning the validity of the Arrhenius kinetics with an average temperature in one-dimensional ZND modeling of detonation initiation and propagation.

In the 1950's, Reingold and Viaud [28] studied detonation propulsion. Their studies were based on Roy's proposal [29] and discussed a design on the stabilization

of combustion in supersonic flow. Several researchers, such as Nicholls et al. [30] and Gross [31, 32, 33], also studied standing detonation waves with the idea of using them for scramjets. With the developing availability of diagnostics with improved temporal and spatial resolutions and powerful computing methods, progress in detonation studies after the 1960's has been overwhelming. It became possible to visualize the ignition process behind a reflected shock wave and discover two different types of shock-induced ignition of a reactive gas known as strong and mild ignition [34].

From the early 1970's, the results of experiments on detonation initiation, propagation and transition made possible the extraction of important criteria. The characteristic size in the structure of a detonation wave, known as the detonation cell size was discovered to be representative parameter for the detonability of a mixture. These data supported that notion that the cell size is a function of the initial pressure, temperature, mixture composition and tube diameter. These all had important implications in the development of detonation engines.

1.2.2 Review of Cycle Analysis of PDEs

More recent research in detonation area comprises of experiments, fundamental analysis of pulse detonation cycle. Identifying the physics of PDEs is a significant key to understand and use this type of engine. Humphrey [1] in 1909 proposed that the heat addition process is isochoric. This approximation of the Chapman–Jouguet process has been regularly employed as a surrogate for the PDE cycle to simplify cycle analysis [2, 5, 35, 36, 37].

It is now understood that the Humphrey cycle may not be appropriate. The so-called Fickett–Jacobs (FJ) cycle [38] may be considered as a modification of the Humphrey cycle. Instead of an isochoric compression, the volume of the compression process is decreased until it reaches the upper CJ state. Even though the FJ cycle is a

more accurate representation of a PDE cycle than the Humphrey cycle, the FJ cycle is also more complex. This cycle model has been used by many researchers [4, 39].

Even though the FJ model was proposed as an improvement over the Humphrey cycle, it also fails to account for the physics based on the subsequent development of the ZND theory. Instead of reaching the CJ state directly, the ZND theory is a two-step process consisting of shock compression along the inert Hugoniot to the ZND state and a subsequent chemical energy release to the CJ state. This ZND cycle may be called the PDE cycle in some studies and has also been used [5, 6, 37].

1.3 Background

1.3.1 Detonation

Cycle analysis of PDEs requires an understanding of CJ theory. The detonation wave travels supersonically into the unreacted gas mixture, with infinitely fast chemistry occurring within the shock. The solution of the one-dimensional conservations equations from the initial state to the reactive Hugoniot yields only two possible final states, known as the upper and lower CJ points [40, 41, 42]. Of interest in this study is the upper CJ point which represent a stable detonation solution. The Hugoniot curve, Rayleigh line, and the CJ points are shown in the Figure 1.1.

Based on thermodynamic properties and conservation conditions, the Hugoniot curve can be described by

$$\tilde{p} = \frac{(\gamma+1) - (\gamma-1)/\tilde{\rho} + 2(\gamma-1)\alpha}{(\gamma+1)/\tilde{\rho} - (\gamma-1)} \tag{1.1}$$

where 1 and 2 represent the upstream and downstream states, $\tilde{p} = p_2/p_1$, $\tilde{\rho} = \rho_2/\rho_1$ and where the dimensionless heat release $\alpha = q\rho_1/p_1$, q being the actual heat release. The inert Hugoniot is given by $q = 0$ and the reactive Hugoniot by a positive value of q.

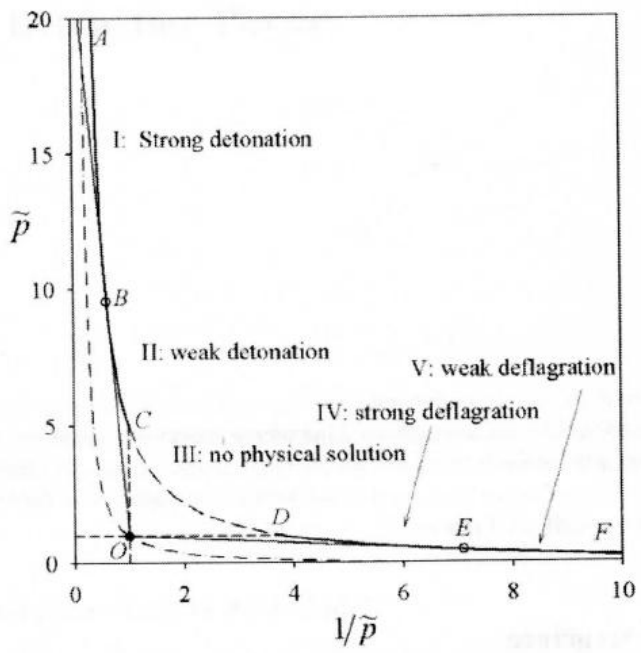

Figure 1.1. Hugoniot showing final states for combustion waves.

1.3.2 Pulse Detonation Engines

A pulse detonation engine uses a repetitive cycle of detonation waves to combust fuel and oxidizer mixture for producing thrust. The idealized engine consists of a shock tube that is open at one end and closed at the other. Fuel and oxidizer are injected into this tube and mixed at the region near the close end. The mixture is ignited to create a detonation wave that travels along the tube toward the open end. This process produces a rise in temperature and pressure. Thrust is generated when gas expands and leaves the shock tube. These processes can be summarized in Figure 1.2.

Theoretically, PDEs can be operated from rest to hypersonic flight speeds [4]. Due to the near-constant-volume operational cycle of PDE, it provides higher thermodynamic efficiency when compared to the conventional, constant pressure, Brayton cycle. Furthermore, two practical advantages over conventional engines are in-

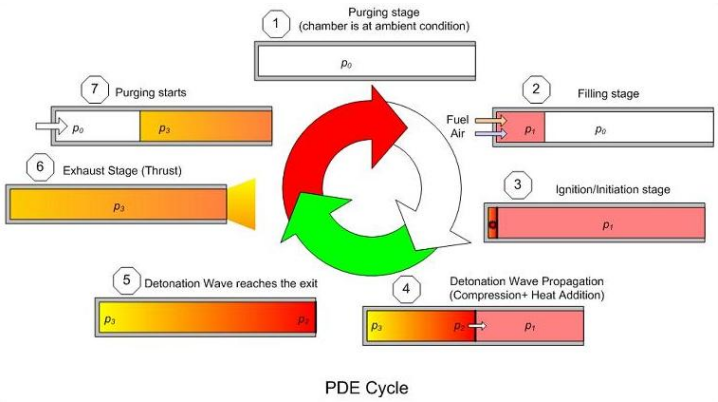

Figure 1.2. Pulse detonation engine cycle. *Source: University of Texas at Arlington Aerodynamics Research Center (ARC); retrieved October 28, 2010 from http://arc.uta.edu/research/pde.htm.*

creased thrust-to-weight ratio and reduced complexity because the detonation wave compresses the mixture without additional turbomachinery devices. Due to these reasons, the geometry of a PDE is considerably simpler. Additionally, the manufacturing process will likely be simpler than conventional engines. Currently, there is no practical PDE that has been put into production; however, several research programs have been ongoing for several years and many ground demonstrator engines have been operated.

1.3.2.1 Parametric Analysis of Ideal PDEs

Cycle analysis is the study of the thermodynamic characteristics of the fluid that flows through a thermodynamic system. For engine studies, cycle analysis is generally divided into two types, namely, parametric and performance analyses. Parametric analysis is commonly used as a tool to determine the performance of aero-engines at various flight conditions [6]. The main objective of this analysis is to relate engine performance parameters to design choice, design limitation and flight environment. Parametric cycle analysis can be further subdivided into ideal and non-ideal analysis.

Generally, parametric analysis of the ideal engine is performed first because of its simplicity. Ideal engine parametric cycle analysis provides results to set an upper limit or the maximum value of engine performance; further, it can be extended to non-ideal cycle analysis when losses of the engine components are included.

In the proposed work, the turbojet engine without afterburner is selected as a model of the study. The engine performance parameters are the specific thrust $F/\dot{m}_0$, the fuel/air ratio f, the specific fuel consumption S and the thermal, propulsive, and overall efficiencies. In the case that the compressor pressure ratio π_c is equal to unity, the ramjet engine is selected instead of the turbojet engine.

1.3.2.2 Parametric Analysis of Non-Ideal PDEs

In the previous section, idealizations and assumptions were applied for basic parametric analysis. In order to add realism, losses of the engine components and the variation of the specific heats have to be included. The calculation of engine performance parameters and efficiencies of the non-ideal engine are similar to the ideal engine but contains more complexity. In this case, the parameters of the non-ideal turbojet are the specific thrust $F/\dot{m}_0$, the fuel/air ratio f, the specific fuel consumption S and the thermal, propulsive, and overall efficiencies as we used in the parametric analysis of ideal PDEs.

CHAPTER 2

EXAMINATION OF THE VARIOUS CYCLES FOR PDE

2.1 The Shock Compression Process for PDE Applications

Without attempting an esoteric discussion of nonequilibrium thermodynamics, consider instead an engineering approach, limiting consideration to conditions expected in PDEs. Consider a shock wave propagating through a nonreactive mixture and a reactive mixture at an incident Mach number of 4.82 which corresponds to a speed of 1600–1800 m/s depending on the gas. This Mach number is typical of those due to propagating detonation waves. Data obtained from the NASA Chemical Equilibrium Application (CEA) code [43] for the downstream state with the gases initially at STP are displayed in Table 2.1. The first four rows for nonreactive gas mixtures show that the downstream states for either the equilibrium or frozen assumption are practically the same. It is next surmised that the approach to the final state occurs via LTE, that is, the path is along the shock hugoniot. This surmise has some support through consideration of the reactive mixture. The mixture first attains a state dictated by the ZND theory which is along the inert hugoniot. This step is similar to that of the nonreactive mixtures and yields the frozen condition. Next, the reactive mixture attains equilibrium through heat release.

2.2 Thermodynamic Cycle Analysis

While cycle analysis generally considers a generic working fluid, a specific reactant mixture and initial conditions are used here to facilitate the comparison. Consider a stoichiometric air and oxygen mixture initially at STP. Equilibrium condi-

Table 2.1. Downstream conditions assuming equilibrium or frozen flow.

Gas	P (bar)		T (K)		h (kJ/kg)	
	Equilibrium	Frozen	Equilibrium	Frozen	Equilibrium	Frozen
Air	27.913	27.897	1509.84	1513.01	1349.44	1349.21
$O_2 + N_2$	27.899	27.883	1505.50	1508.61	1357.99	1357.75
$He + O_2 + N_2$	28.152	28.130	1599.42	1603.59	1624.98	1624.57
$Ar + O_2 + N_2$	28.152	28.130	1599.42	1603.59	1295.12	1294.80
$H_2 + O_2 + N_2$	15.835	27.814	2946.48	1531.15	1354.86	1873.74

tions are obtained from the NASA CEA code [43] while nonequilibrium chemistry is obtained via Cantera [44]. Figure 2.1 concludes the three ideal processes under discussion in both the p–v and T–s diagrams, portraying the total (or stagnation) states. The initial state of the reactants is (1). The hugoniot running through (1) is shown in Fig. 2.2 as a dashed line. The post-detonation hugoniot is also shown in the figure by another dashed line. This hugoniot was obtained using data obtained from the NASA CEA code [43], yielding a dimensionless heat release $\alpha = q\rho_1/p_1 = 27.28$.

2.2.1 Thermodynamic Cycle Analysis Based on the Humphrey Cycle

The Humphrey cycle is the simplest model for a PDE by assuming that the compression process is an isochoric one [5, 35, 36]. It consists of an isochoric compression, an isentropic expansion and a fictitious isobaric process to close the cycle. This simplification is obvious in a p–v diagram (Fig. 2.2). For example, the post-compression state is not the CJ state as would be expected. This cycle underpredicts the performance of PDE.

Hydrogen and air are chosen as fuel and oxidizer respectively. The initial condition is set at STP (101 kPa, 300 K, and 1.1727 m^3/kg). As shown in the p–v diagram, the pressure increases isochorically to intersect the reactive Hugoniot given

by the dimensionless heat release α, Eq. (1.1). The subsequent isentropic expansion reduces the pressure to the ambient level. The cycle is closed to the initial state by a fictitious isobaric process. In the T–s diagram, the temperature starts with the compression process which based on the ideal gas law

$$PV = nRT \tag{2.1}$$

The specific entropy Δs also increases following the equation of specific entropy in constant volume process

$$\Delta s = C_v \ln (T_2/T_1) \tag{2.2}$$

The isentropic expansion that follows reduces the temperature. The final isobaric process to close the cycle decreases both T and s. The entropy drop is given by

$$\Delta s = C_p \ln (T_2/T_1) \tag{2.3}$$

The necessary values, which consists of R, C_v and C_p can be found by using the Cantera/Hugoniot relation.

As shown in Fig. 2.2, the gas, initially at (1) is compressed isochorically to state (2H) where $p_{2H} = 0.8$ MPa and $T_{2H} = 2550$ K. The gas then expands isentropically to reach (3H) where $p_{3H} = 0.1$ MPa and $T_{3H} = 1520$ K. The increase in entropy from (1) to (3H) is $\Delta s = 3.08$ kJ/(kg $\cdot$ K). The cycle is closed by a fictitious isobaric process (3H) $\rightarrow$ (1) of heat rejection to the open ambient conditions. A single value of specific heat ratio $\gamma = 1.242$ appears sufficient for such an analysis but with $R = 348$ kJ/(kg $\cdot$ K) and 396 kJ/(kg $\cdot$ K) for the isochoric compression and for the isentropic expansion respectively.

2.2.2 Thermodynamic Cycle Analysis Based on the FJ Cycle

The FJ cycle, as can be seen in Fig. 2.3, consists of a compression and heat addition process that brings the gas from state (1) to state (2CJ). This process is strictly a nonequilibrium one. Recall that the CJ theory assumes an instantaneous heat release (unlike the more elaborate ZND theory). Within the one-dimensional model of the detonation process, this process is identical to Rayleigh heating and thus can be regarded to be a process that is in local thermodynamic equilibrium [45, 46]. In other words, the tangent from (1) to (2CJ) in the p–v diagram is the same path as that of Rayleigh heating. Isentropic expansion occurs between (2CJ) and (3CJ) after which the cycle is closed by a fictitious isobaric process to the initial state.

Specifically for a hydrogen–air mixture initially at STP, $p_{2CJ} = 1.5$ MPa and decreases the specific volume to $v_{2CJ} = 0.67$ m^3/kg with the same dimensionless heat release $\alpha = 27.28$ as for the Humphrey cycle. The isentropic expansion from (2CJ) to (3CJ) yields $p_{3CJ} = 0.1$ MPa and $v_{3CJ} = 5.92$ m^3/kg respectively. Finally, a fictitious isobaric process returns both pressure and specific volume to the initial state.

While the calculations of (p_{2CJ}, v_{2CJ}) are straightforward, (T_{2CJ}, s_{2CJ}) are more complicated to determine. The value of the gas constant changes from (1′) to (2CJ) as, for example, in computations using Cantera [44]. For simplicity, a linear variation of R between the value at state (1′) and (2CJ) is accurate for modeling the nonequilibrium heat release, which coincided with the equilibrium Rayleigh heat release. The temperature rises to 2920 K and the entropy rises by 3.12 kJ/(kg $\cdot$ K). The gas then expands isentropically from (2CJ) to (3CJ). State (3CJ) is different from state (3H) because the isentropic expansions arise from the different states (2CJ) and (2H) state, respectively. The values of p_{3CJ}, v_{3CJ} and T_{3CJ} are 0.1 MPa, 5.922 m^3/kg and 1562 K respectively.

For cycle analysis, the tangency relationship had to be used to evaluate the CJ point exactly, namely,

$$
\begin{aligned}
v_{CJ} \;=\; & \Big\{\frac{1}{4}[1+\gamma-\gamma^2-3\gamma^3-2\alpha(1-3\gamma-\gamma^2+3\gamma^3) \\
& -v_1(-2+4\gamma^2-2\gamma^3+2\alpha(-1+\gamma^2)-(-1+3\gamma^2)v_1)] \\
& ((-3-\gamma+5\gamma^2+\gamma^3+2\alpha(-1+\gamma^2)+2\alpha(1-3\gamma-\gamma^2+3\gamma^3)-(-1+3\gamma^2)v_1)^2 \\
& -4(-3-2\gamma-2\gamma^2-4\gamma^3-4\alpha(-1-\gamma+\gamma^2+\gamma^3) \\
& +(2\gamma^2+2\gamma^3)v_1)(-1+\gamma+\gamma^2-\gamma^3-2\alpha(-1+3\gamma-3\gamma^2+\gamma^3) \\
& +v_1(-2\gamma^2+2\gamma^3+2(1-\gamma-\gamma^2+\gamma^3)(\alpha+v_1))))\Big\} \\
& \big/\big[-3-2\gamma-2\gamma^2-4\gamma^3-4\alpha(-1-\gamma+\gamma^2+\gamma^3)+(2\gamma^2+2\gamma^3)v_1\big]
\end{aligned}
\tag{2.4}
$$

(Details are found in Appendix B.) This is because the CJ point from an equilibrium calculation, say, using CEA is slightly different from that obtained from a nonequilibrium one, say, using Cantera. Thus, for simplicity, a tangent is cast from the inert to the reactive hugoniot whose intersection is the CJ point.

A similar difficulty is encountered in evaluating T_{CJ} due to the variation of the gas constant R from the initial point. It was found that a linear variation of value of R from (1) to (2CJ) is satisfactory to describe this path in the T–s diagram, which is necessary for cycle analysis for the same reason as above. In summary, the properties at (2CJ) are a total pressure of 1.5 MPa, a total specific volume of 0.67 m^3/kg, a total temperature of 2920 K and an increase of entropy to 3.12 $\mathrm{kJ/kg \cdot K}$. The CJ cycle then allows the gas to expand isentropically to (3CJ). The properties here at a total pressure of 0.1 MPa, a total specific volume of 5.92 m^3/kg, a total temperature of 1515 K.

2.2.3 Thermodynamic Cycle Analysis Based on Zel'dovich–von Neumann–Döring Cycle

Although the FJ model was proposed as an improvement over the Humphrey cycle, it fails to account for the physics espoused by the ZND model because shock compression does not increase the pressure directly to the CJ point; however, it compresses the pressure to the ZND point. This process acts along the inert Hugoniot. The next step is the ZND→CJ transition with heat release due to chemical reactions. The two-step process of the ZND model is shown in Fig. 2.4 by (1) → (1′) → (2CJ) as described previously. There are no ambiguities in determining (1′) for a real mixture. Calculations using Cantera yield total postshock pressure and specific volume as 2.8 MPa and 0.22 m^3/kg respectively. The subsequent CJ value is the same as the FJ cycle reported above. This is followed by the same isentropic expansion as the FJ cycle, followed by a fictitious isobaric process to close the cycle. Moreover, the shock compression to the ZND point raises the temperature to 1531 K with an entropy increase to 1.366 kJ/(kg · K). The heat addition that brings the gas from the ZND to the CJ point raises the temperature to 2920 K with a further increase of entropy to 3.12 kJ/(kg · K). From Cantera, the gas constant at these two points are 397.6 and 348.22 kJ/(kg · K) respectively. The isentropic expansion to 1 atm lowers the gas temperature to 1515 K. Finally, a fictitious isobaric process closes the cycle.

It is now proposed that the work in a ZND cycle is split into a part that is not available and another that is available, these being known as internal and external work respectively. Consider a shock wave as shown in Fig. 2.2.3. States (1) and (1′) in the figure refer to the same states as in Fig. 2.2. Figure 2.2.3 shows an isentropic expansion to state (4) which is shown in Fig. 2.2 by a dotted line. Now, for the control volume to remain stationary, a force must be exerted to equal the change in momentum flux from (1) to (4) with $p_4 = p_1$. In other words, thrust work must be

done which is equal to the area enclosed by the path (1) $\underset{\text{shock}}{\rightarrow}$ (1′) → (4) → (1) in Fig. 2.2. This is known as internal work which imparts internal energy to sustain the shock and is unavailable for work production.

Turning next to a detonation wave as shown in Fig. 2.2.3, the process now includes the heat release from (1′) to (2CJ) in the induction zone followed by an isentropic expansion to state (3CJ). The total work available is equal to the area enclosed by the path (1) $\underset{\text{isen}}{\rightarrow}$ (1′) → (2CJ) → (3CJ) → (1). However, based on the above discussion, a certain portion of the work is unavailable. Only the difference in the areas of the two paths in Fig. 2.2 is available, this being known as the external work.

2.2.4 Comparison Between the Humphrey, FJ, ZND Cycles

A consideration of the thermodynamics of the Humphrey, FJ and ZND cycles reveals that drastic assumptions are made for all of them to gain some tractability. Of these, it is suggested that the ZND cycle models the actual PDE engine with the proper physics. To summarize, for engineering analysis, we examine the discrepancies in cycle performance due to the three models. The net work out, net heat in and the efficiency are given respectively by

$$w_{out} = \oint P_t \, dv \tag{2.5a}$$

$$q_{t,in} = \oint T_t \, ds \tag{2.5b}$$

$$\eta = w_{out}/q_{t,in} \tag{2.5c}$$

where the subscript t is used to indicate that the total property is being considered. Note that while the same Eq. (2.5a) is used for the three cycles, the ZND cycle requires that the internal work be neglected. Evaluating the above equations yield results displayed in Table 2.2. Note that these are cyclic values. A peculiarity of

Table 2.2. Performance comparisons of the three cycles.

	Humphrey	Fickett–Jacobs	Zel'dovich–von Neumann–Döring
Work out (MJ/kg)	0.709	0.834	1.40
Heat in (MJ/kg)	1.07	1.3	2.29
Efficiency (%)	66.5	64.3	61.2

pulse detonation engines is that the cyclic values are likely much larger than the time-averaged values, the latter being dependent on the number of cycles per unit time. When the time required for the fill and purge processes are included, then performance parameters such as *power* or *thrust*, depending on whether the engine is used for power production or for propulsion, will be lower than if the two aforementioned processes are ignored. Nonetheless, this extra complication has no bearing to cycle analysis.

From these results, it can be stated that the ZND cycle accounts for the internal energy in the shock wave while the Humphrey and FJ cycles only account for heat addition. The results point out that the performance parameters are largely underestimated in Humphrey and FJ cycles, which may have a drastic effect on performance analysis.

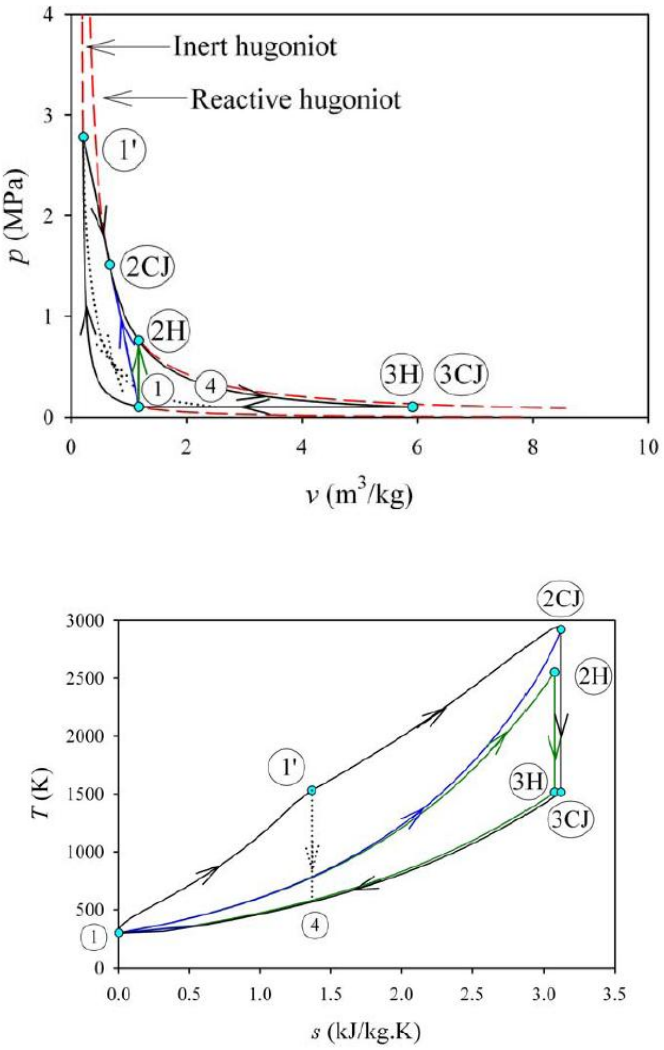

Figure 2.1. Comparison between ideal Humphrey ($1 \rightarrow 2H \rightarrow 3H \rightarrow 1$), FJ ($1 \rightarrow 2CJ \rightarrow 3CJ \rightarrow 1$) and ZND ($1 \rightarrow 1' \rightarrow 2CJ \rightarrow 3CJ \rightarrow 1$) cycles for a stoichiometric hydrogen/air mixture initially at STP..

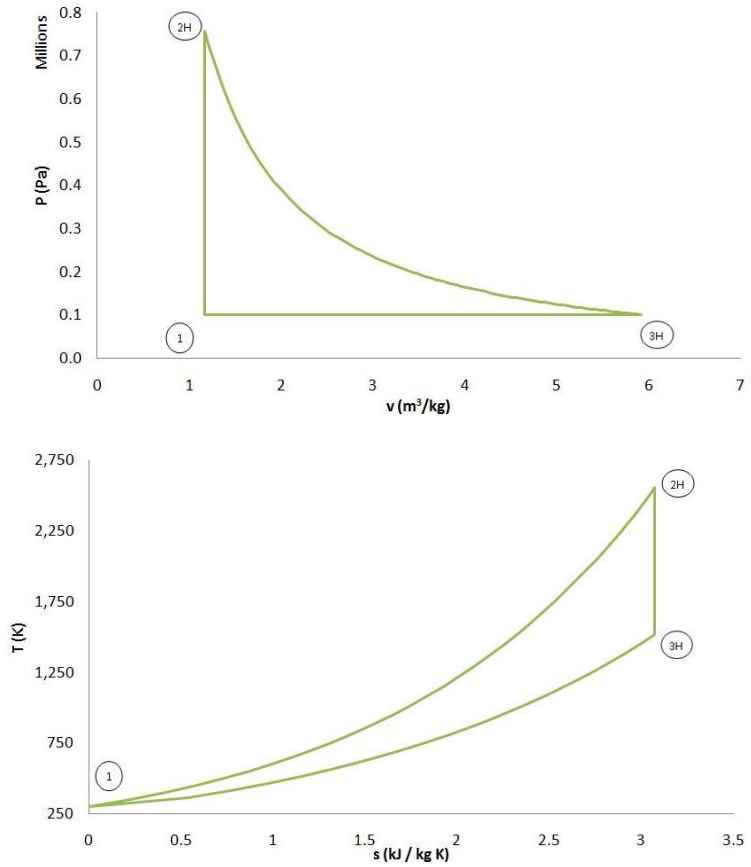

Figure 2.2. The Humphrey process.

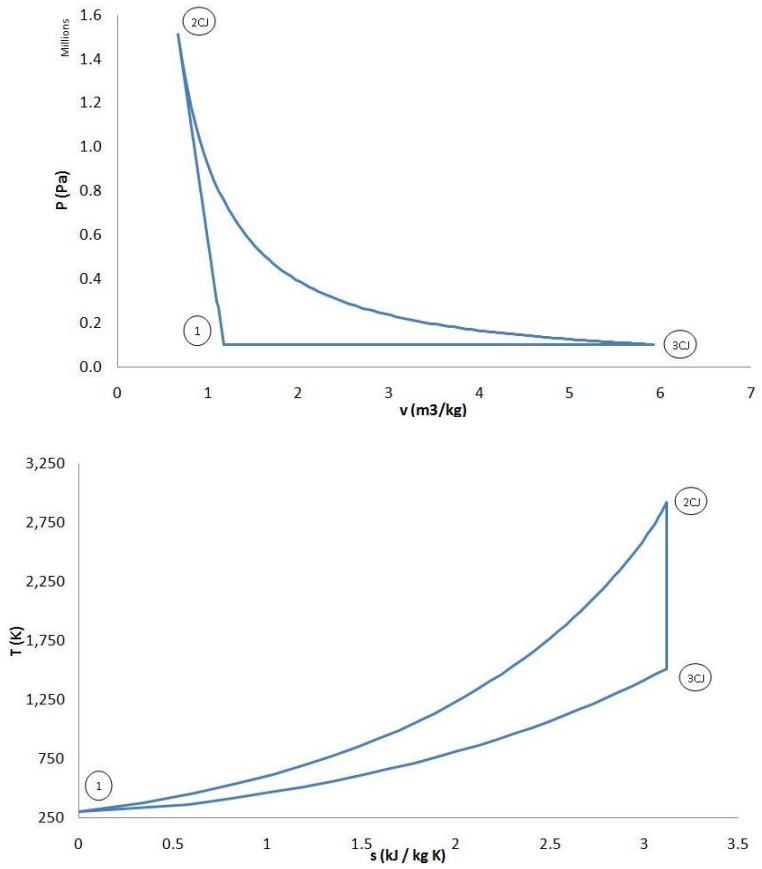

Figure 2.3. The Fickett-Jacobs process.

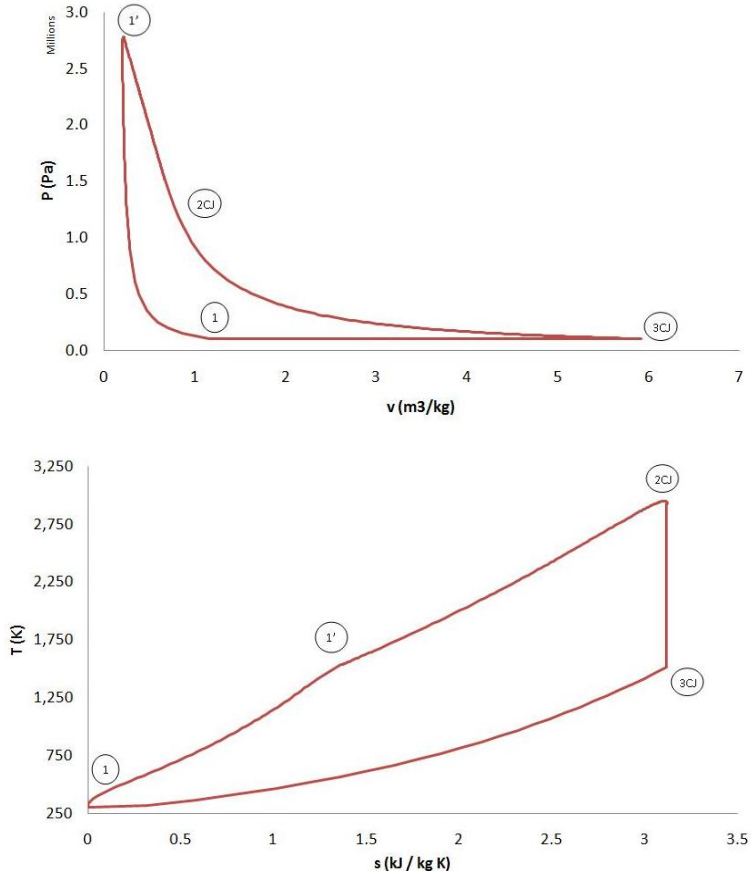

Figure 2.4. The Zel'dovich–von Neumann–Döring process.

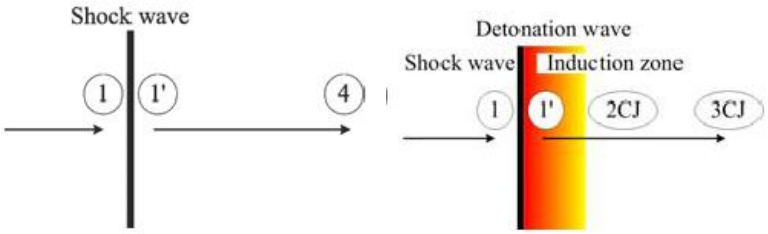

Figure 2.5. The two-step ZND process for a detonation wave.

CHAPTER 3

PRECOMPRESSION, ARBITRARY HEAT RELEASE AND UNSTEADY GASDYNAMIC PROPERTIES OF ZND CYCLE

3.1 Precompression

As a general statement, all heat engines using compressible substances as the working medium require that the substance be compressed before heat addition. Shock compression by itself may be sufficient to initiate and perhaps sustain cyclic operation although no such practical devices are known to exist. Instead, it is suggested here that sustained cyclic operation requires precompression. For a detonation engine, this precompression need not be large, unlike conventional engines, thus ensuring that the overall compression does not exceed structural and material limits. The effect of a small amount of precompression is considered, with compressor pressure ratios $\pi_c = 1$–3 for a hydrogen–air mixture initially at STP. At a compression ratio of 1, the engine is defined as a ramjet/PDE; otherwise, it is considered as a turbojet/PDE. The reference values that are used in the calculation such as specific heat γ, nondimensional heat release parameter α, and the specific heat capacities, C_p and C_v, can be retrieved and calculated from the Cantera/Hugoniot relation [44]. The reference and calculated values of each cycle are shown in the Table 3.1.

The results are shown in Fig. 3.1 and Table 3.2. The cycle work remains fairly constant but the heat input increases with increasing compression. The results show that the cycle efficiency decreases slightly with increasing compression.

Table 3.1. The reference and calculated values of ZND cycle for stoichiometric hydrogen–air mixture initially at STP with precompression

π_c	γ_1	γ_2	$\frac{\alpha}{Pv}$	C_p [kJ/(kg · K)]	C_v [kJ/(kg · K)]	P_2 (MPa)	P_3 (MPa)	P_4 (MPa)	T_2 (K)	T_3 (K)	T_4 (K)
1	1.319	1.242	27.28	1.65×10^3	1.25×10^3	2.29	1.26	0.101	1225	2114	1292
1.5	1.317	1.242	24.39	1.66×10^3	1.25×10^3	3.27	1.75	0.101	1318	2249	1292
2	1.316	1.242	23.22	1.66×10^3	1.26×10^3	4.47	2.30	0.101	1411	2399	1307
2.5	1.315	1.241	21.14	1.66×10^3	1.26×10^3	5.30	2.67	0.101	1490	2500	1324
3	1.314	1.241	20.09	1.66×10^3	1.26×10^3	6.40	3.13	0.101	1575	2625	1348

Table 3.2. Performance of ZND cycle for stoichiometric hydrogen–air mixture initially at STP with precompression

$\pi_c =$	1	1.5	2	2.5	3
Work out (MJ/kg)	1.40	1.45	1.45	1.45	1.42
Heat in (MJ/kg)	2.29	2.49	2.62	2.70	2.76
Efficiency (%)	61.2	58.5	55.6	53.7	51.5

3.2 Arbitrary Heat Release

Finally, instead of a specific reactant mixture, an arbitrary heat release is considered here. The nondimensional heat release α ranges from 10 to 30, which covers most reactant mixtures of interest for PDEs. Figure 3.2 shows the ZND cycles for this range of α with a precompression ratio $\pi_c = 3$. The work out and heat in per cycle and the cyclic efficiency are listed in Table 3.3. Not surprisingly, the more energetic fuel yields a higher cycle efficiency.

Table 3.3. Performance of ZND cycle for different arbitrary values of nondimensional heat release of a reactive mixture initially at STP.

$\alpha =$	10	15	20	30
Work out (MJ/kg)	0.521	1.06	1.42	2.81
Heat in (MJ/kg)	1.03	1.97	2.76	5.02
Efficiency (%)	50.5	53.7	51.5	56.0

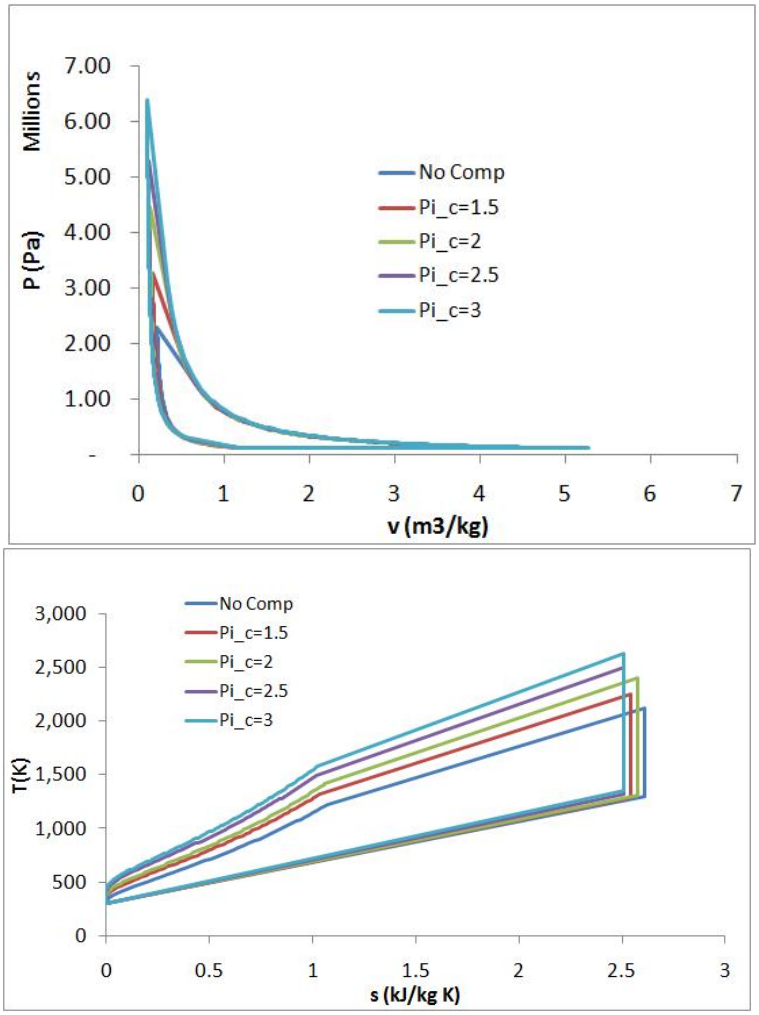

Figure 3.1. ZND cycle with precompression. Isentropes not shown for clarity.

3.3 Unsteady Gasdynamic Properties

Due to the unsteady gasdynamic behavior of PDEs, the performance analysis of PDEs contains more complexity than other types of aero engine. For a thrust-producing engine, the unsteady exhaust has to be more carefully understood. As in previous analytical studies, unsteadiness of the inlet is ignored. Endo and Fujiwara [47, 48] proposed an analytical formulation for the duration of the shock in PDE tube. The equations that were used to determine the time at which detonation wave reaches open end of PDE tube $t_{plateau}$ are

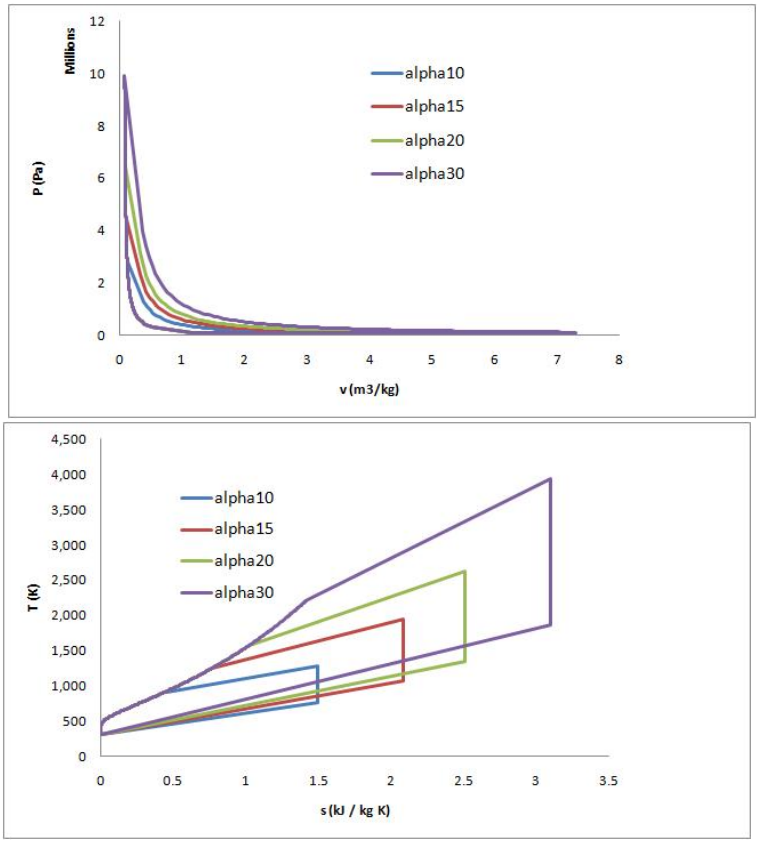

Figure 3.2. ZND cycle with arbitrary heat release with $\pi_c = 3$. Isentropes not shown for clarity.

$$k_I = \frac{\gamma_2 + 1}{2\gamma_2} \tag{3.1}$$

$$k_{II} = \frac{\gamma_2 - 1}{2\gamma_2} \tag{3.2}$$

$$k_{III} = \frac{k_I}{k_{II}} \tag{3.3}$$

$$k_{IV} = \frac{2[(\gamma_2 k_I)^{k_{III}} - 1]}{\gamma_2 k_{II}} \tag{3.4}$$

$$k_V = 2k_I^{-k_{III}/2} \tag{3.5}$$

The k_I–k_V are constants which can be determined by γ_2 only. After k_V is retrieved, we need to determine time at which detonation wave breaks out from the open end of the PDE t_{CJ} in order to calculate $t_{plateau}$. The t_{CJ} is a relation between tube length and Chapman–Jouguet detonation speed of detonable gas mixture V_{CJ}.

$$t_{CJ} = \frac{L}{V_{CJ}} \tag{3.6}$$

Finally, $t_{plateau}$ can be determined by

$$t_{plateau} = k_V t_{CJ} \tag{3.7}$$

Based on this model, the $t_{plateau}$ can be calculated. In this case, the frequency of detonation wave is set as 100 Hz and the length of tube is equal to 1 m at compressor pressure ratio equals to 1, 1.5, 2, 2.5, and 3. From these assumption, the average pressure and temperature in the tube, P_4 and T_4 can be calculated. The results from Endo and Fujiwara model are shown in Table 3.4.

Table 3.4. The average $t_{plateau}$, exhaust pressure and temperature from the detonation chamber

$\pi_c =$	1	1.5	2	2.5	3
$t_{plateau}$ (s)	0.00164	0.00168	0.00167	0.00167	0.00167
Average P_4 (kPa)	199.77	242.16	294.03	328.23	368.07
Average T_4 (K)	1530	1580	1630	1680	1730

From Table 3.4, the average temperature is around 1500–1730 K, which will be exhausted to the turbine. Generally, the turbine can tolerate a temperature up

to around 2500 K due to material limitations. So, this cycle can be operated safely operated with existing turbine materials and cooling techniques.

CHAPTER 4

PARAMETRIC ANALYSIS OF A PDE/TURBOJET

4.1 Parametric Analysis of Ideal PDEs

Ideal parametric analysis is considerably less complicated than so-called real analysis. The result from ideal thermodynamics cycle analysis can be used as an upper limit or the maximum value; further, it can be extended to the real cycle analysis when losses of the engine are included. This parametric analysis contains of performance parameters which are specific thrust, fuel/air ratio, and specific fuel consumption; and efficiencies which are thermal, propulsive, and overall efficiencies. The equations that were used for parametric analysis of ideal PDEs are

$$\tau_r = 1 + \frac{(\gamma - 1)}{2} M_0^2 \tag{4.1}$$

$$\tau_\lambda = \frac{T_{t4}}{T_0} \tag{4.2}$$

$$\tau_c = \pi_c^{(\gamma-1)/\gamma} \tag{4.3}$$

$$\tau_t = 1 - \frac{\tau_r}{\tau_\lambda}(\tau_c - 1) \tag{4.4}$$

$$\frac{V_9}{a_0} = \sqrt{\frac{2}{\gamma - 1}\frac{\tau_\lambda}{\tau_r \tau_c}(\tau_r \tau_c \tau_t - 1)} \tag{4.5}$$

$$F/\dot{m}_0 = a_0 \left(\frac{V_9}{a_0} - M_0 \right) \tag{4.6}$$

$$f = \frac{c_p T_0}{h_{PR}}(\tau_\lambda - \tau_r \tau_c) \tag{4.7}$$

$$S = \frac{f}{F/\dot{m}_0} \tag{4.8}$$

$$\eta_T = \frac{(1 + f)(V_9^2/2) - V_0^2/2}{f h_{PR}} \tag{4.9}$$

$$\eta_P = \frac{2M_0}{V_9/a_0 + M_0} \tag{4.10}$$

$$\eta_O = \eta_T \eta_P \tag{4.11}$$

The compressor pressure ratio π_c = 1–3 which includes the simpler ramjet case when $\pi_c = 1$. The results of the parametric analysis of ideal PDEs are plotted in Figures 4.1–4.2 in terms of the compressor pressure ratio and in Figures 4.3–4.4 in terms of the flight Mach number which varied from 0 to 5.

For the Figure 4.1(a), there is no specific thrust at M_0=0 and π_c=1. This poor performance can be overcome when the compressor is added to the engine. The addition of compressor-turbine unit can improve the specific thrust as shown. The specific thrust is maximized at M_0=3; after that, specific thrust is decreased at M_0 more than 4. This characteristic acts similar to the ideal turbojet engine [6] at the same region(π_c=1–3). In the Figure 4.1(b), the decrease in fuel/air ratio is occurred with increasing of M_0 due to the increase in the total temperature entering the combustor when M_0 is increased. Figure 4.1(c) demonstrates that increasing of π_c will decrease the specific fuel consumption because specific thrust is increased when π_c is increased. In the Figure 4.2, the efficiencies which are thermal, propulsive, and overall efficiencies are shown versus the π_c at M_0=0-5. For the thermal and overall efficiencies (Figure 4.2(a) and Figure 4.2(c)), the efficiencies are increased with increasing of π_c and M_0. For the propulsive efficiency which is shown in Figure 4.2(b), the efficiency cannot be determined at M_0=0. The propulsive efficiency is decreased with increasing of π_c; however, when M_0 is increased, the efficiency is also increased.

Figures 4.3 and 4.4 illustrate another representation of the data in Figures 4.1 and 4.2. The performance parameters and efficiencies are plotted with M_0 in Figures 4.3 and 4.4. Figure 4.3(a) shows that the specific thrust is increased when M_0 is

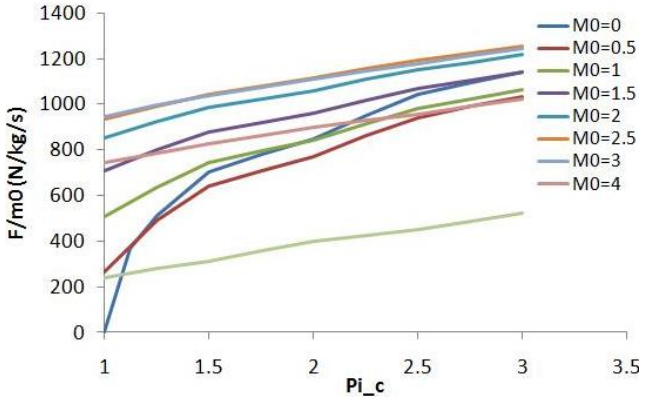

(a)

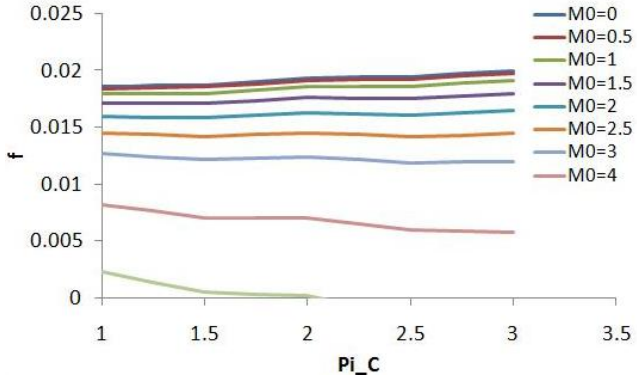

(b)

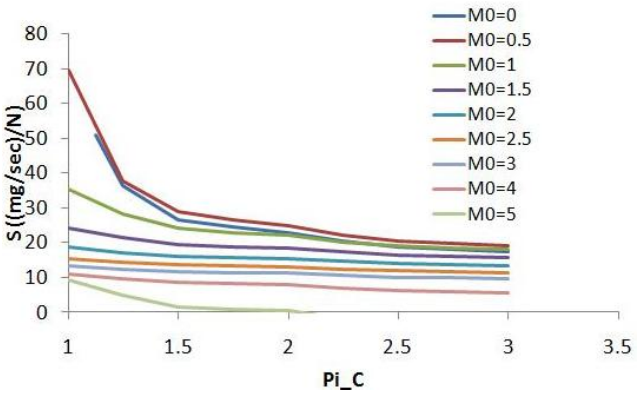

(c)

Figure 4.1. Performance Parameters of Ideal Turbojet/PDEs for $\pi_c = 1$–3; (a) Specific thrust with compressor pressure ratio, (b) Fuel/air ratio with compressor pressure ratio, (c) Specific fuel consumption with compressor pressure ratio .

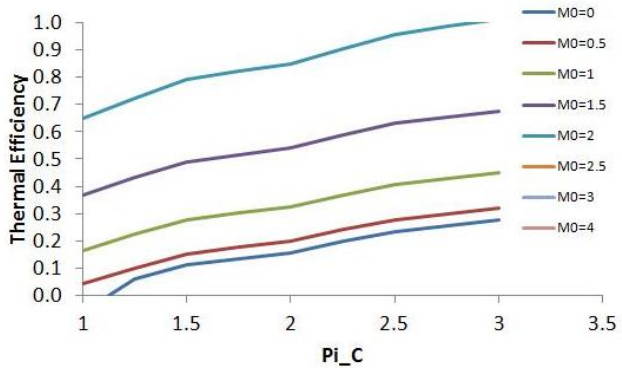

(a)

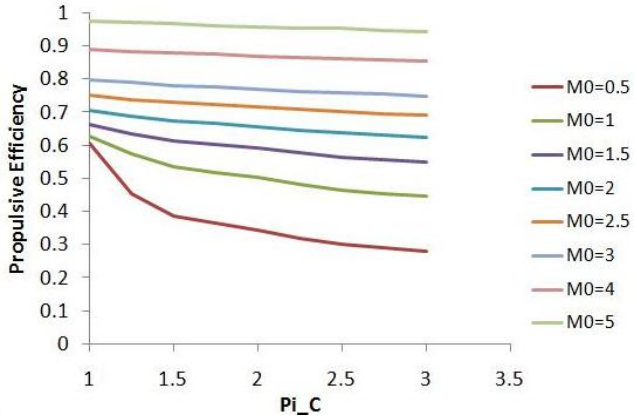

(b)

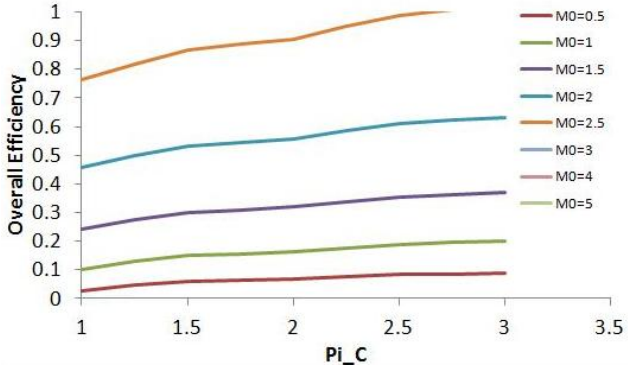

(c)

Figure 4.2. Efficiencies of Ideal Turbojet/PDEs for $\pi_c = 1$–3; (a) Thermal efficiency with compressor pressure ratio, (b) Propulsive efficiency with compressor pressure ratio, (c) Overall efficiency with compressor pressure ratio.

increased from 0–3 and it is decreased when M_0 is more than 3. So, we can conclude that the engine is desirable for M_0 around 0–3 at π_c = 1–3. In Figure 4.3(b), the decreasing of fuel/air ratio with the increasing of M_0 at the region of π_c = 1–3 is shown. The plotting of specific fuel consumption with M_0, which is shown in Figure 4.3(c), demonstrates that the specific fuel consumption is increased with increasing of M_0 from $M_0 = 0$ to around 0.5; after that, the specific fuel consumption is decreased with increasing of M_0 and π_c. For the efficiencies, Figure 4.4 illustrates the general increase in thermal, propulsive, and overall efficiencies when M_0 is increased.

4.2 Parametric Analysis of Non-Ideal PDEs

In the previous section, idealizations and assumptions were applied in basic parametric analysis. In order to achieve realistic values, losses in the engine and variation of specific heat have to be included. So, calculation of the engine performance parameters and efficiencies of non-ideal turbojet engine introduces realism but contains more complexity. The equations that were used to determine the parametric analysis of non-ideal turbojet/PDEs are illustrated in Eq. 4.12–4.28. These equations can provide performance parameters which are specific thrust, fuel/air ratio, and specific fuel consumption; and efficiencies which are thermal, propulsive, and overall efficiencies.

$$\tau_r = 1 + \frac{(\gamma_c - 1)}{2} M_0^2 \tag{4.12}$$

$$\tau_\lambda = \frac{c_{pt} T_{t4}}{c_{pc} T_0} \tag{4.13}$$

$$\tau_c = \pi_c^{(\gamma_c - 1)/\gamma_c e_c} \tag{4.14}$$

$$\eta_c = \frac{\pi_c^{(\gamma_c - 1)/\gamma_c}}{\tau_c - 1} \tag{4.15}$$

$$\tau_t = 1 - \frac{1}{\eta_m (1 + f)} \frac{\tau_r}{\tau_\lambda} (\tau_c - 1) \tag{4.16}$$

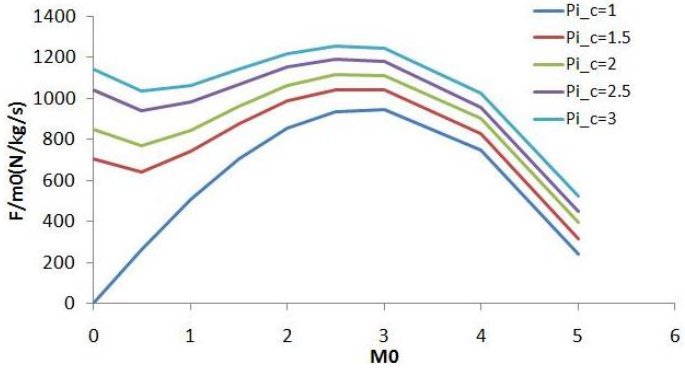

(a)

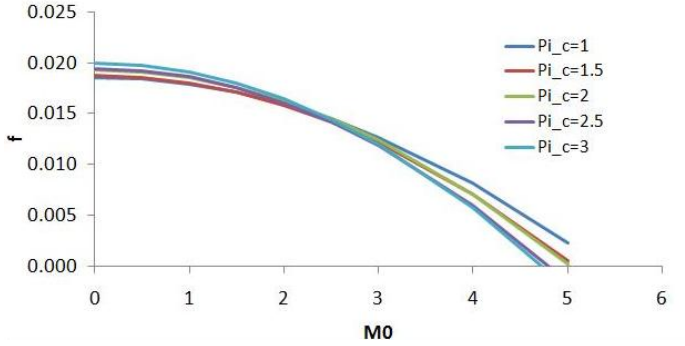

(b)

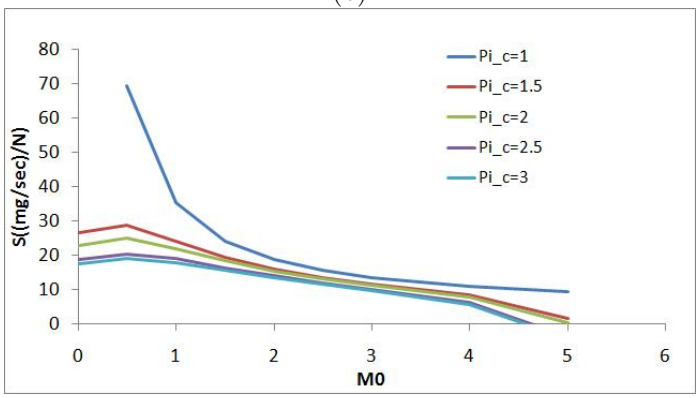

(c)

Figure 4.3. Performance Parameters of Ideal Turbojet/PDEs for $M_0 = 0$–5; (a) Specific thrust with flight Mach number, (b) Fuel/air ratio with flight Mach number, (c) Specific fuel consumption with flight Mach number.

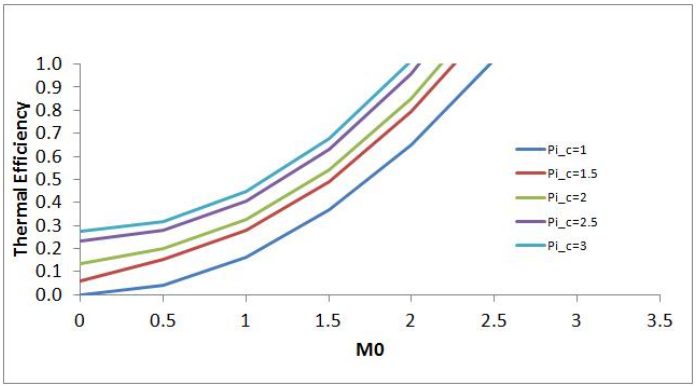

(a)

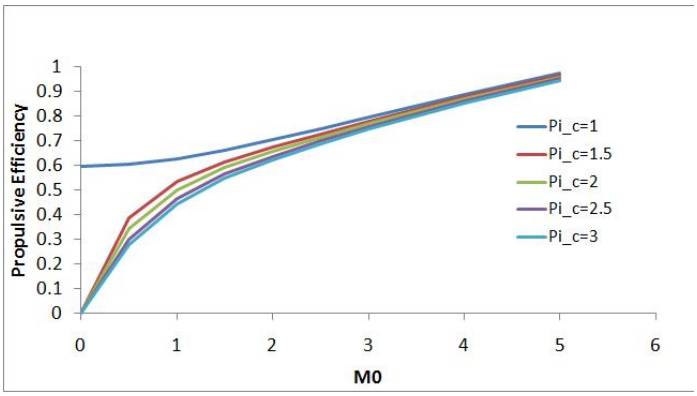

(b)

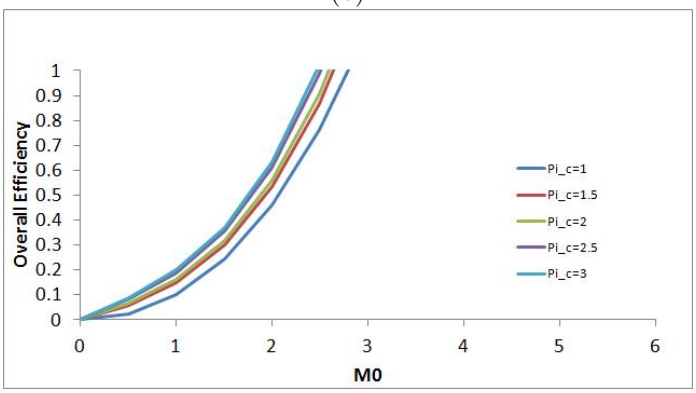

(c)

Figure 4.4. Efficiencies of Ideal Turbojet/PDEs for $M_0 = 0$–5; (a) Thermal efficiency with flight Mach number, (b) Propulsive efficiency with flight Mach number, (c) Overall efficiency with flight Mach number.

$$\pi_t = \tau_t^{\gamma_t/[(\gamma_t-1)e_t]} \tag{4.17}$$

$$\eta_t = \frac{1-\tau_t}{1-\tau_t^{1/e_t}} \tag{4.18}$$

$$\frac{P_{t9}}{P_9} = \pi_r \pi_d \pi_c \pi_b \pi_n \pi_t \tag{4.19}$$

$$M_9 = \sqrt{\frac{2}{\gamma_t - 1}\left[\frac{P_{t9}}{P_9}^{(\gamma_t-1)/\gamma_t} - 1\right]} \tag{4.20}$$

$$\frac{T_9}{T_0} = \frac{\tau_\lambda \tau_t}{\frac{P_{t9}}{P_9}^{\frac{(\gamma_t-1)}{\gamma_t}}} \frac{c_{pc}}{c_{pt}} \tag{4.21}$$

$$\frac{V_9}{a_0} = M_9 \sqrt{\frac{\gamma_t R_t T_9}{\gamma_c R_c T_0}} \tag{4.22}$$

$$F/\dot{m}_0 = a_0(1+f)\left(\frac{V_9}{a_0} - M_0 + (1+f)\frac{R_t \frac{T_9}{T_0}}{R_c \frac{V_9}{a_0}} \frac{(1-\frac{P_0}{P_9})}{\gamma_c}\right) \tag{4.23}$$

$$f = \frac{\tau_\lambda - \tau_r \tau_c}{\frac{h_{PR}\eta_b}{c_{pc}T_0} - \tau_\lambda} \tag{4.24}$$

$$S = \frac{f}{F/\dot{m}_0} \tag{4.25}$$

$$\eta_T = \frac{(1+f)(V_9^2/2) - V_0^2/2}{f h_{PR}} \tag{4.26}$$

$$\eta_P = \frac{2V_0(F/\dot{m}_0)}{a_0^2[(1+f)(\frac{V_9}{a_0})^2 - M_0^2]} \tag{4.27}$$

$$\eta_O = \eta_T \eta_P \tag{4.28}$$

The results of the parametric analysis of non-ideal PDEs can be plotted as shown in the Figure 4.5–4.8. At first, we analyze the performance parameters and efficiencies with variation of compressing ratio from 1–3 which shown in Figures 4.5–4.6

From Figure 4.5(a), the plotting shows that at the specific thrust is increased with increasing of π_c the region around M_0 = 0–2; after that at M_0 is more than 2, specific thrust is not increased when π_c is increased. In this Figure, the region of

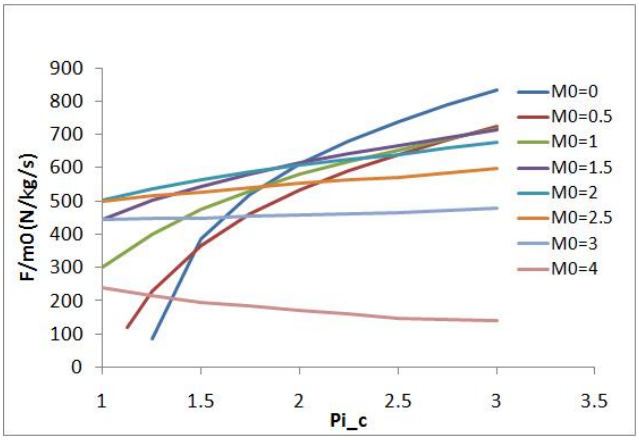

(a)

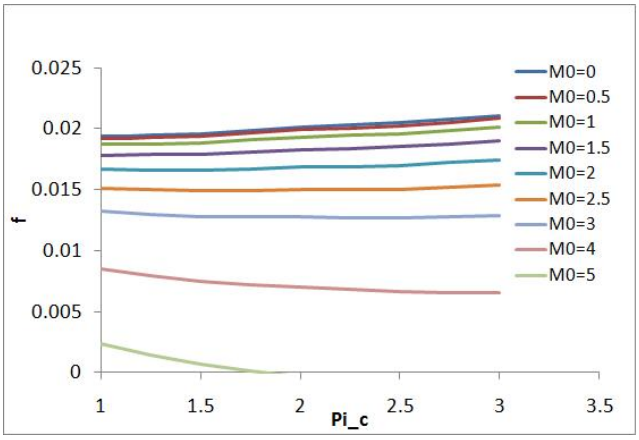

(b)

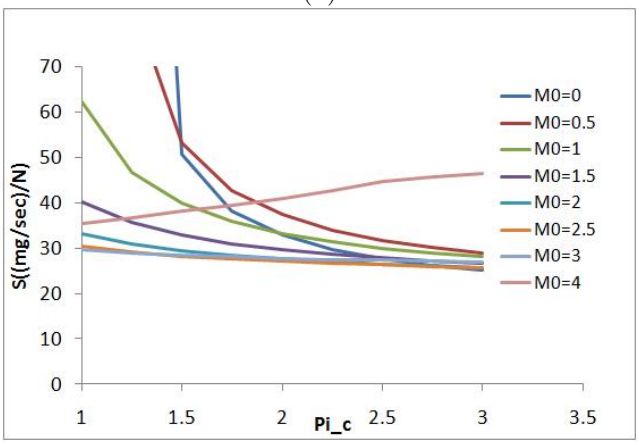

(c)

Figure 4.5. Performance parameters of non-ideal Turbojet/PDEs for $\pi_c = 1$–3; (a) Specific thrust with compressor pressure ratio, (b) Fuel/air ratio with compressor pressure ratio, (c) Specific fuel consumption with compressor pressure ratio.

low M_0 and π_c does not have thrust. Furthermore, at the high Mach number (M_0 more than 4), the specific thrust cannot be presented due to the effect of the losses. Comparing specific thrust of non-ideal PDEs (Figure 4.5(a)) to specific thrust of ideal PDEs (Figure 4.1(a)), we can see that the specific thrust of the non-ideal PDEs is lower than the ideal one due to losses in the engine. In the ideal PDEs, there is no specific thrust when π_c =1 and M_0 =0. In the non-ideal PDEs, the thrust cannot be presented at both the low M_0 and π_c and high M_0. From Figure 4.5(b), fuel/air ratio is decreased with increasing of M_0. Comparing fuel/air ratio of non-ideal PDEs (Figure 4.5(b)) to fuel/air ratio of ideal PDEs (Figure 4.1(b)), we can see that the fuel/air ratio of a non-ideal engine is slightly larger than the ideal one due to the increasing of specific heat across the combustor. The specific fuel consumption, which is shown in Figure 4.5(c), is decreased when π_c is increased. Furthermore, at the high Mach number (M_0 more than 4), the specific fuel consumption also cannot be presented due to the effect of the losses. Comparing specific fuel consumption of non-ideal PDEs (Figure 4.5(c)) to specific fuel consumption of ideal PDEs (Figure 4.1(c)), the specific fuel consumption of non-ideal engine is slightly larger than the ideal one. The main reason for this increase in specific fuel consumption is the increasing of fuel/air ratio.

The thermal, propulsive, and overall efficiencies of a non-ideal PDE are plotted with π_c in Figure 4.6. In Figure 4.6(a), the thermal efficiency is increased when π_c is increased at the region M_0 = 0–3; however, the efficiency is decreased when π_c is increased at M_0 more than 3 due to the decreasing of specific thrust. This result is similar to the thermal efficiency of the non-ideal turbojet [6]. Comparing thermal efficiency of non-ideal PDEs (Figure 4.6(a)) to thermal efficiency of ideal PDEs (Figure 4.2(a)), the efficiency of the non-ideal engine is smaller than the ideal one as to be expected. The propulsive efficiency of non-ideal PDEs, which is shown in Figure 4.6(b), acts similar to the ideal PDEs. The efficiency is decreased with

increasing of π_c; and it is increased when M_0 is increased. However, the value of propulsive efficiency of non-ideal PDEs is a little larger than the ideal one. The reason is the decrease of exhaust velocity. For the overall efficiency, which is illustrated in Figure 4.6(c), the trend is similar to the thermal efficiency. Comparing overall efficiency of non-ideal PDEs (Fig. 4.6(c)) to overall efficiency of ideal PDEs (Figure 4.2(c)), the efficiency of non-ideal engine is smaller than the ideal one due to the decrease of thermal efficiency.

After we analyze the performance parameters and efficiencies with variation of compressing ratio from 1–3 (Figures 4.5–4.6), we will consider these parameters with flight Mach number which varied from 0–5. However, for high Mach numbers, some parameters cannot be presented due to the effect of the losses especially at high π_c. Figures 4.7–4.8, which are plotted versus flight Mach number, may represent only flight Mach number from 0–4 for these cases.

Figures 4.7 and 4.8 illustrate another representation of the data in Figures 4.5 and 4.6. The performance parameters and efficiencies are plotted with M_0 in these Figures (4.7 and 4.8). In Figure 4.7(a), at π_c= 1–2, the specific thrust is increased when M_0 is increased from 0–2; and it is decreased when M_0 is more than 2. Further, the specific thrust is increased when M_0 is increased from 0–1.5 and it is decreased when M_0 is more than 1.5 at π_c more than 2. Comparing specific thrust of non-ideal PDEs (Figure 4.7(a)) to specific thrust of ideal PDEs (Figure 4.3(a)), we can see that the specific thrust of the non-ideal PDEs is lower than the ideal one due to losses in the engine; especially in the high Mach number region, the specific thrust rapidly decreased when M_0 is increased. So, we can conclude that the engine is desirable for M_0 around 0–2 at π_c = 1–2; and, the engine is desirable for M_0 around 0–1.5 at π_c more than 2. In Figure 4.7(b), the decreasing of fuel/air ratio with the increasing of M_0 at the region of π_c = 1–3 is shown. Comparing fuel/air ratio of non-ideal

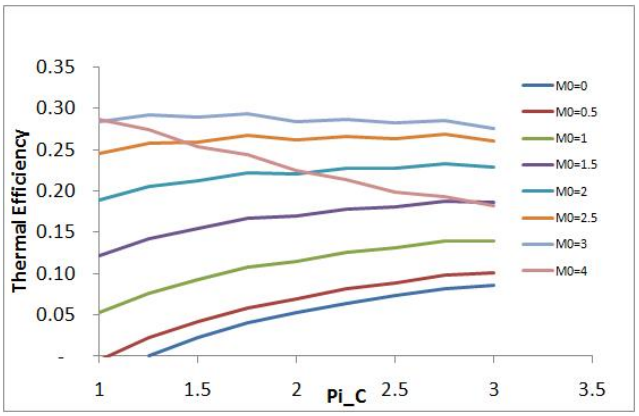

(a)

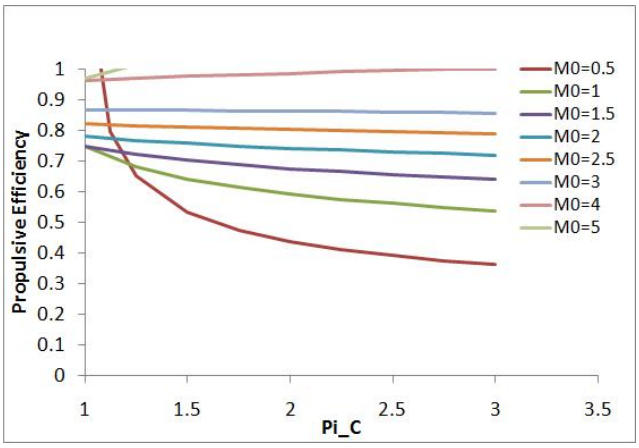

(b)

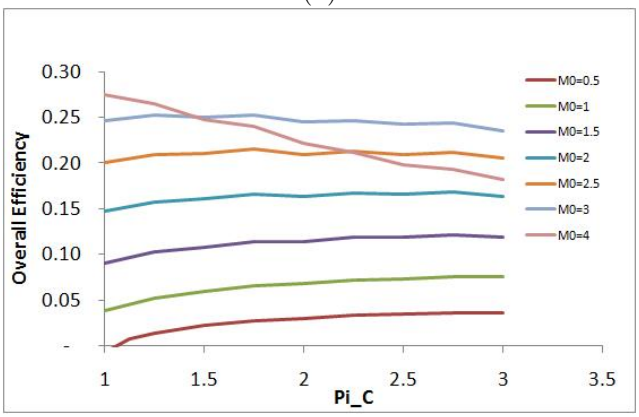

(c)

Figure 4.6. Efficiencies of non-ideal Turbojet/PDEs for π_c = 1–3; (a) Thermal efficiency with compressor pressure ratio, (b) Propulsive efficiency with compressor pressure ratio, (c) Overall efficiency with compressor pressure ratio.

PDEs (Figure 4.7(b)) to fuel/air ratio of ideal PDEs (Figure 4.3(b)), the value of fuel/air ratio of non-ideal engine is a little larger than the ideal one because of the increasing of specific heat across the combustor. The Figure 4.7(c) demonstrates the specific fuel consumption with M_0. The specific fuel consumption is increased with increasing M_0 from 0 to around 0.5; after that from $M_0 = 0.5$ to around 3, the specific fuel consumption is decreased with increasing of M_0. Subsequently, for $M_0 > 3$, the specific fuel consumption is increased with the increasing of M_0 again. This characteristic is similar to the non-ideal turbojet engine in that the specific fuel consumption is increased again at high Mach number especially when π_c is high [6]. Comparing specific fuel consumption of non-ideal PDEs (Figure 4.7(c)) to specific fuel consumption of ideal PDEs (Figure 4.3(c)), the value is larger than the latter due to the increasing of fuel/air ratio.

For the thermal efficiencies, Figure 4.8(a) illustrates that the thermal efficiency is increased when M_0 is increased. However, at the high Mach number region, which are M_0 more than 3.5 where π_c= 1–2 and M_0 more than 3 where π_c more than 2, thermal efficiency is decreased when M_0 is increased. Comparing thermal efficiency of non-ideal PDEs (Figure 4.8(a)) to thermal efficiency of ideal PDEs (Figure 4.4(a)), the efficiency is smaller than the latter especially at the high Mach number as mentioned.

The propulsive efficiency of non-ideal PDEs, which is shown in Figure 4.8(b), acts similar to the ideal PDEs. The efficiency is increased when M_0 is increased. Comparing propulsive efficiency of non-ideal PDEs (Figure 4.8(b)) to propulsive efficiency of ideal PDEs (Figure 4.4(b)), the efficiency of non-ideal engine is slightly larger than the ideal one due to the decreasing of exhaust velocity. For the overall efficiency, which is illustrated in Figure 4.8(c), the trend is similar to the thermal efficiency. Comparing overall efficiency of non-ideal PDEs (Figure 4.8(c)) to overall

efficiency of ideal PDEs (Figure 4.4(c)), the efficiency is smaller than the latter due to the decreasing of thermal efficiency.

4.3 Comparison of the Performance Between a Turbojet and a PDE/Turbojet

To verify that the PDE provides better performance than the turbojet, the efficiency of both propulsion systems is compared in this section. Due to the difference between the characteristics of ZND and Brayton cycle, both cycles cannot be directly compared. The ZND cycle mainly compresses the reactants by the shock wave along the inert Hugoniot curve; however, the Brayton cycle uses a compressor to increase the pressure and temperature. There are many attempts to compare these two different cycles. In 2002, Heiser and Pratt [5] compared performance parameters of PDEs with turbojets by setting the compression static temperature rise ratio to be equal. This method was also used by Wu et al. [37] to compare ideal PDE with Humphrey and Brayton cycles. In the same year, Hutchins and Metghalchi [35] discussed the efficiency and effectiveness between Humphrey and Brayton cycles by assuming the equality of compression ratio. In 2006, Wintenberger and Shepherd [39] proposed the comparison of thermal efficiency of the FJ cycle with the Humphrey and Brayton cycles. They explained that the comparison can be based on two possibilities. The first one is a function of compression ratio as by Hutchins and Metghalchi [35]. Another possibility is a function of combustion pressure ratio (peak combustion pressure).

In this study, we set the range of compressor pressure ratio from 5 to 50 for the turbojet. We assign the T_3 of Brayton cycle in two cases, T_3=1600 and 2900 K. The first case is assigned due to the limitation of engine material; the second one is assigned because we try to set the efficiencies of the Brayton cycle to be equal to the ZND cycle. However, the material will not withstand such a high temperature unless additional precautions are implemented. The results from these two cases of Brayton

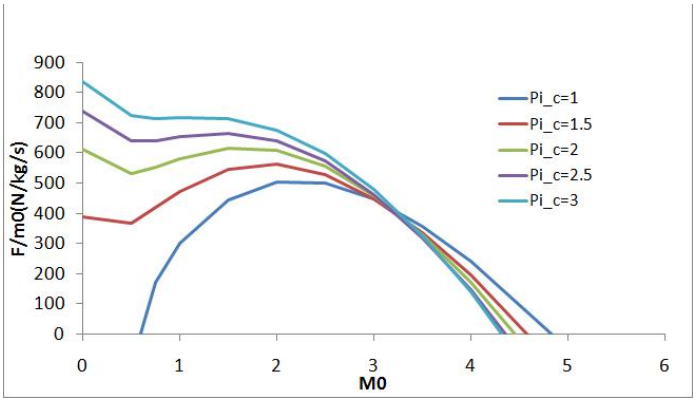

(a)

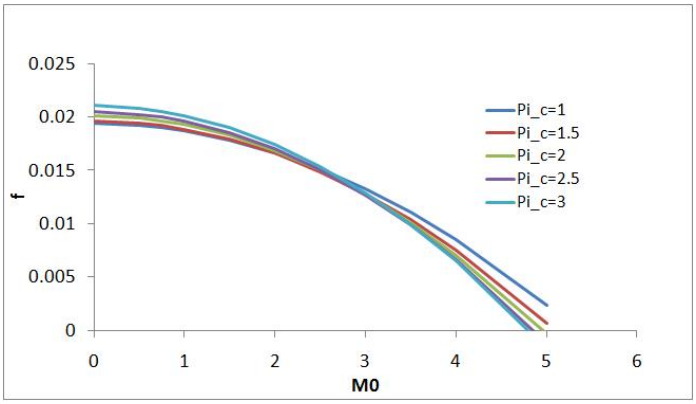

(b)

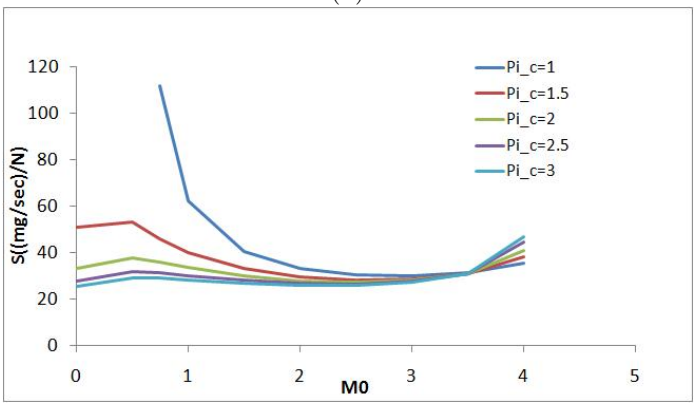

(c)

Figure 4.7. Performance parameters of Non-ideal Turbojet/PDEs for $M_0 = 0$–5; (a) Specific thrust with flight Mach number, (b) Fuel air ratio with flight Mach number, (c) Specific fuel consumption with flight Mach number.

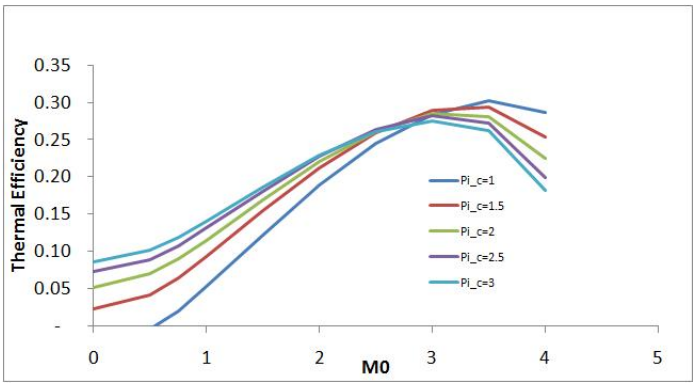

(a)

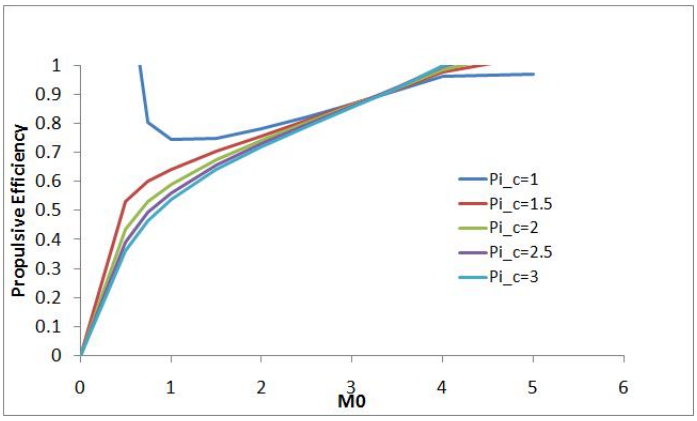

(b)

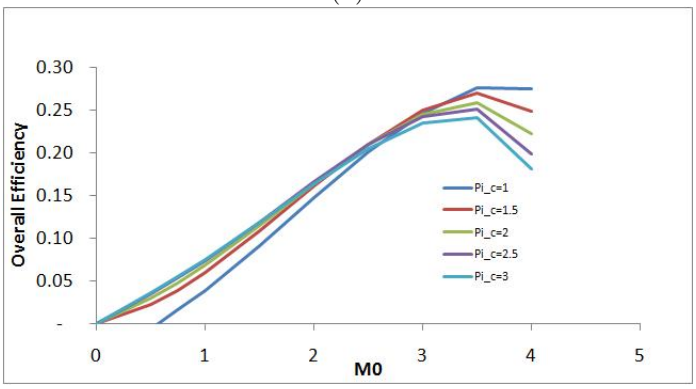

(c)

Figure 4.8. Efficiencies of Non-ideal Turbojet/PDEs for M_0 = 0–5; (a) Thermal efficiency with flight Mach number, (b) Propulsive efficiency with flight Mach number, (c) Overall efficiency with flight Mach number.

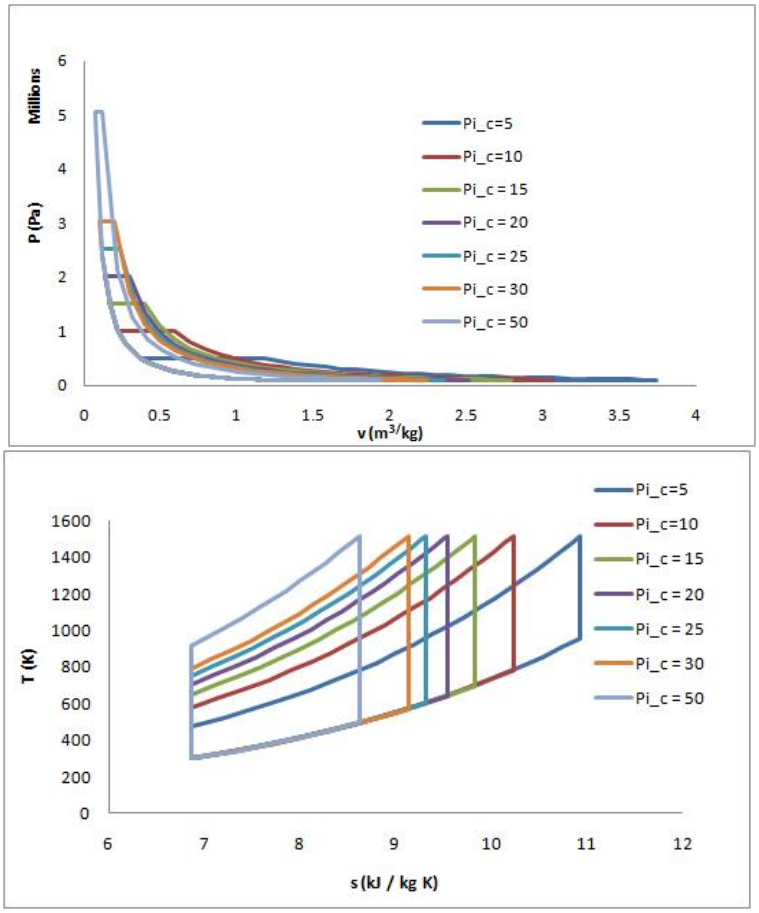

Figure 4.9. The Brayton process: $T_3 = 1600$ K.

cycle and ZND cycle are compared in terms net work done, specific heat input, and efficiency as shown in the Tables 4.1 and4.2.

From Figure 4.9, we can calculate the net work done, specific heat input, and efficiency of this cycle. The results are described in the Table 4.1. The net work done is around 0.53-0.63 MJ/kg. The specific heat input is around 1.34-1.63 MJ/kg. The efficiency is around 39-41 %.

For $T_3 = 2900$, the p–v and T–s diagram are shown in Figure 4.10.

Table 4.1. Performance of Brayton cycle for stoichiometric hydrogen–air mixture initially at STP with precompression at $T_3 = 1600$ K

π_c	Net work done (MJ/kg)	Specific heat input (MJ/kg)	Efficiency(%)
5	0.526	1.341	39
10	0.618	1.578	39
15	0.654	1.630	40
20	0.647	1.628	40
25	0.640	1.604	40
30	0.629	1.571	40
50	0.583	1.407	41

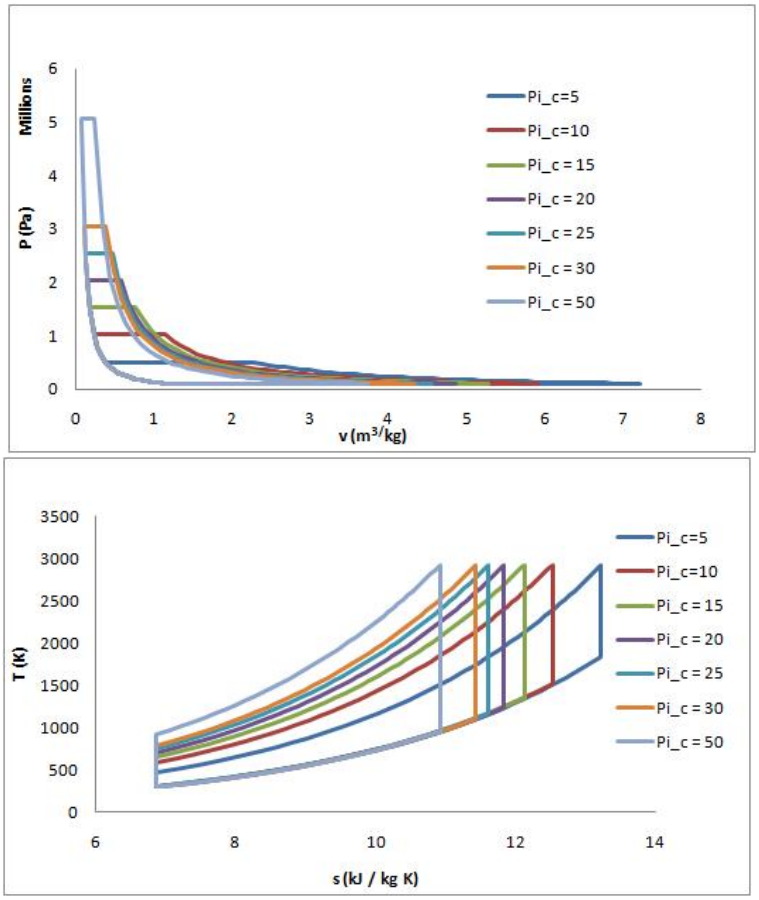

Figure 4.10. The Brayton process: $T_3 = 2900$ K.

Table 4.2. Performance of Brayton cycle for stoichiometric hydrogen–air mixture initially at STP with precompression at $T_3 = 2900$ K

π_c	Net work done (MJ/kg)	Specific heat input (MJ/kg)	Efficiency(%)
5	1.247	3.154	40
10	1.557	3.949	39
15	1.695	4.279	40
20	1.758	4.599	38
25	1.798	4.562	39
30	1.832	4.628	40
50	1.875	4.717	40

From Figure 4.10, we can calculate the net work done, specific heat input, and efficiency of Brayton cycle with $T_3 = 2900$ K as shown in Table 4.2. The net work done is around 1.25-1.88 MJ/kg. The specific heat input is around 3.15–4.72 MJ/kg. The efficiency is around 38–40 %. Comparing the results from Brayton cycle with $T_3 = 1600$ K in Table 4.1 with Brayton cycle with $T_3 = 2900$ K in Table 4.2, the net work done at $T_3 = 2900$ K is higher than $T_3 = 1600$ K. However, the specific heat input at $T_3 = 2900$ K is also higher than $T_3 = 1600$ K. So, the efficiency between $T_3 = 1600$ and 2900 K are similar.

The results from the Brayton cycle with both $T_3 = 1600$ and 2900 K can be compared with the net work done, specific heat input, and efficiency of ZND cycle as shown in Table 3.2. This comparison clarifies the potential for mechanical work between these cycles. The detonation process in the ZND cycle have a potential to produce work more than the Brayton cycle, the constant pressure process. Further, the specific heat input of the ZND cycle is lower than the Brayton cycle. The advantages of the the detonation process over the constant pressure process come from the repetitive cycle of detonation waves that combust fuel and oxidizer mixture for

producing thrust. The detonation wave, that travels along the tube in PDEs, produces a rise in temperature and pressure without additional turbomachinery devices. However, there is the work in the ZND cycle that is not available which can be called the internal work as mention in section 2.2.3. This internal work imparts internal energy to sustain the shock and is unavailable for producing work. Even subtract this internal work from the net work done of the ZND cycle, this cycle provide better efficiency that Brayton cycle. However, in comparing different combustion modes, we cannot assigned the π_c to be equal and directly compare them. We have to use data in Tables 3.2, 4.1, and 4.2 to analyze the efficiency of ZND cycle that consists of π_c=1–3 and Brayton cycle that consists of π_c=5–50 in both cases, T_3 = 1600 and 2900 K. The comparison obviously shows that the ZND cycle provides better work and efficiency even operated in the lower compressor pressure ratio.

CHAPTER 5

SUMMARY AND CONCLUSIONS

In this study, an evaluation of the relative merits and shortfalls of three different models for engineering analysis of pulse detonation engines was briefly given. While simple to implement, the constant volume, or Humphrey, cycle does not adequately capture the physics of the detonation phenomenon to provide a realistic estimate of the work. A more sophisticated model to account for the pressure rise in a detonation wave, known as the Fickett–Jacobs model, also underestimates the work. Finally, the Zel'dovich–von Neumann–Döring model was deemed to be the most appropriate. This requires an assumption of local thermodynamic equilibrium in the shock process. It was found that the heat addition process can be modeled by a supersonic Rayleigh heating process. Additionally, it was suggested that the shock causes a certain amount of work to be unavailable. The analysis was performed using a stoichiometric hydrogen–air mixture initially at STP. Inclusion of precompression revealed that the efficiency decreases with compressor pressure ratio. A generic heat addition process was also considered. In this case, it was found that an energetic material with higher heat release yields an increased thermodynamic efficiency.

In addition, the study on engine performance parameters and efficiencies can be used to indicate the performance of the turbojet/PDE. The performance parameters and efficiencies were obtained for compressor pressure ratios of 1–3 and freestream Mach numbers of 1–5 for both ideal and non-ideal PDEs are analyzed. The results from both engines are different especially at a region of high compressor pressure ratio and flight Mach number due to losses of the engine and variation of specific heat. In

the last section, a conventional Brayton cycle with compressor pressure ratio between 5 to 50 is brought as a reference for comparing against a with turbojet/PDE. The results obviously point out that the turbojet/PDE provides better efficiency even the operated compressor pressure ratio is lower.

5.1 Future Work

Even though this study is based on assigned initial conditions, it can be modified to deal with other initial conditions in a further study. The present model of the turbojet engine without afterburner can be changed to other types of engines such as with afterburning or with bypass. The type of fuel that used can be also changed by adjusting the value of h_{PR}. The initial conditions such as pressure, temperature, or specific volume are also able to assigned values that vary from this condition in the thermodynamic cycle analysis, i.e., a performance analysis can be performed as well. Furthermore, for the non-ideal PDEs, some aspects such as the unsteady opening and closing of the PDEs, and heat losses in the combustion chamber are not included in the present analysis. In order to add more realism, these aspects may be applied. However, due to the complexity of these aspects, researches in this area hardly mention about them. These aspects need a further consideration. A further study could also analyze about them.

APPENDIX A

CONFERENCE PAPERS

1. **Vutthivithayarak R**, Braun EM, Lu FK. Examination of the various cycles for pulse detonation engines. *47th AIAA/ASME/SAE/ ASEE Joint Propulsion Conference & Exhibit*, July 31–August 3, 2011, San Diego, California.
2. **Vutthivithayarak R**, Braun EM, Lu FK. On thermodynamic cycles for detonation engines. *28th International Symposium on Shock Waves*, July 17–22, 2011, Manchester, UK.

APPENDIX B

THE RANKINE–HUGONIOT RELATIONSHIP AND THE UPPER CJ POINT

Other than available software such as CEA and Stanjan, the CJ state can also be obtained analytically. The hugoniot in general is given by

$$\frac{p_2}{p_1} = \frac{(\gamma+1) - (\gamma-1)\frac{v_1}{v_2} + (2(\gamma-1)\alpha)}{(\gamma+1)\frac{v_1}{v_2} - (\gamma-1)} \tag{B.1}$$

where $\alpha = q\rho_1/p_1$ is the nondimensional heat release parameter. By definition, the CJ point is located by the tangent from the initial state to the reactive Hugoniot. The slope of the tangent is given by

$$m = \frac{(1-\gamma^2)[(\gamma+1) - (\gamma-1)v_1 + 2(\gamma-1)\alpha]}{(\gamma+1)v_{CJ} - (\gamma+1)} \tag{B.2}$$

Now,

$$m = \frac{p_{CJ} - p_1}{v_{CJ} - v_1} \tag{B.3}$$

Manipulating Eqs. (B.1)–(B.3) yields Eq. (2.4).

REFERENCES

[1] H. A. Humphrey, "An internal-combustion pump, and other applications of a new principle," *Proceedings of the Institution of Mechanical Engineers*, vol. 77, no. 1, pp. 1075–1200, 1909.

[2] T. R. A. Bussing and G. Pappas, *Pulse Detonation Engine Theory and Concepts*, ser. Progress in Aeronautics and Astronautics. Reston, Virginia: AIAA, 1996, vol. 165, pp. 421–472, 26th AIAA Fluid Dynamics Conference, San Diego, California, June 19–22, 1995.

[3] S. Eidelman and X. Yang, "of the pulse detonation engine efficiency," in AIAA Paper 1998–3877, 1998, 34th AIAA/ASME/SAE/ASEE Joint Propulsion Conference and Exhibit, Cleveland, Ohio, July 13–15, 1998.

[4] G. D. Roy, S. M. Frolov, A. A. Borisov, and D. W. Netzer, "Pulse detonation propulsion: Challenges, current status, and future perspective," *Progress in Energy and Combustion Science*, vol. 30, no. 6, pp. 545–672, 2004, doi: 10.1016/j.pecs.2004.05.001.

[5] W. H. Heiser and D. T. Pratt, "Thermodynamic cycle analysis of pulse detonation engine," *Journal of Propulsion and Power*, vol. 18, no. 1, pp. 68–76, 2002.

[6] J. D. Mattingly, *Elements of Propulsion: Gas Turbines and Rockets*. Reston, Virginia: AIAA, 2006.

[7] D. Clerk, *Gas and Oil Engine*, sixth, revised and enlarged ed. London: Longmans, Green and Co., 1896.

[8] J. C. L.C̃ummins, *Internal Fire*. Lake Oswego, Oregon: Carnot Press, 1976.

[9] M. Bertholet, "Sur la vitesse de propagation des phénomènes explosifs dans les gaz," *Comptes Rendus Hebdomadaires des Séances de l'Académie des Sciences*, vol. 93, pp. 18–21, 1881, (On the Velocity of Propagation of Explosive Processes in Gases).

[10] ——, "Sur l'onde explosif," *Comptes Rendus Hebdomadaires des Séances de l'Académie des Sciences*, vol. 94, pp. 149–152, 1882, (On Explosive Waves).

[11] F.-E. Mallard and H. L. Le Chatelier, "Sur la vitesse de propagation de l'inflammation dans les mélanges gazeux explosifs," *Comptes Rendus Hebdomadaires des Séances de l'Académie des Sciences*, vol. 93, pp. 145–148, 1881, (On the Velocity of Propagation from Ignition in Gaseous Explosive Mixtures).

[12] D. L. Chapman, "On the rate of explosion in gases," *Philosophical Magazine Series 5*, vol. 47, no. 284, pp. 90–104, 1889.

[13] W. J. M. Rankine, "On the thermodynamic theory of finite longitudinal distubance," *Philosophical Transactions of the Royal Society of London*, vol. 160, pp. 277–288, 1870. [Online]. Available: http://www.jstor.org/stable/109061

[14] P.-H. Hugoniot, "Mémoire sur la propagation du movement dans les corps et plus spécialement dans les gaz parfaits. premiere partie," *Journal de l'École Polytechnique*, vol. 57, pp. 3–97, 1887, (Memorandum on Bulk Flow Especially of a Perfect Gas. Part I).

[15] ——, "Mémoire sur la propagation du movement dans les corps et plus spécialement dans les gaz parfaits. deuxième partie," *Journal de l'École Polytechnique*, vol. 58, pp. 1–125, 1889, (Memorandum on Bulk Flow Especially of a Perfect Gas. Part II).

[16] M. D. Salas, "The curious events leading to the theory of shock waves," *Shock Waves*, vol. 16, no. 6, pp. 477–487, 2006.

[17] P. Vieille, "Déformation des ondes au cours de leur propagation," *Comptes Rendus Hebdomadaires des Séances de l'Académie des Sciences*, vol. 128, pp. 1437–1440, 1889, (Wave Deformation During Their Propagation).

[18] ——, "Sur les discontinuités produites par la dètente brusque de gaz comprimès," *Comptes Rendus Hebdomadaires des Séances de l'Académie des Sciences*, vol. 129, pp. 1128–1130, 1900, (On the Discontinuities Produced by the Sudden Relaxation of Compressed Gases).

[19] E. Jouguet, "Sur la propagation des réactions chimiques dans les gaz," *Journal des Mathématiques Pures et Appliquées*, vol. 1 and 2, pp. 347–425 and 5–86, 1905 and 1906, (On the Propagation of Chemical Reactions in Gases).

[20] J. N. Johnson and R. Chéret, *Classic Papers in Shock Compression Science.* New York: Springer, 1998.

[21] C. Campbell and D. W. Woodhead, "The ignition of gases by an explosion wave. Part I. Carbon monoxide and hydrogen mixtures," *Journal of the Chemical Society*, pp. 3010–3021, 1926.

[22] W. Payman and H. Robinson, "The pressure wave sent out by an explosive. Part I," Safety in Mines Research Board, Paper 26, 1926.

[23] W. Payman and W. C. F. Shepherd, "The pressure wave sent out by an explosive. Part II," Safety in Mines Research Board, Paper 29, 1927.

[24] W. Payman, "The detonation wave in gaseous mixtures and the predetonation period," *Proceedings of the Royal Society of London Series A*, vol. 120, no. 784, pp. 90–109, 1928. [Online]. Available: http://www.jstor.org/stable/95032

[25] Y. B. Zeldovich, "K teori rasprostranenia detonazi v gasoobrasnikh systemakh," *Zhurnal Experimental'noi i Teoreticheskoi Fiziki*, vol. 10, pp. 543–568, 1940, English translation: On the Theory of the Propagation of Detonation in Gaseous Systems, NACA TM 1261, 1960.

[26] J. von Neumann, "Theory of Detonation Waves. Progress Report to the National Defense Research Committee Div. B, OSRD-549, (April 1, 1942. PB 31090)," in *John von Neumann: Collected Works, 1903–1957*, A. H. Taub, Ed. New York: Pergamon, 1963, vol. 6.

[27] W. Döring, "Über den detonationsvorgang in gasen," *Annalen der Physik*, vol. 43, pp. 421–436, 1943, (On the Detonation Process in Gases); volume renumbered to vol. 435, no. 6.

[28] L. Reingold and L. Viaud, *Perfectionnements apportés aux foyers à circulation interne supersonique, notamment aux chambres de combustion pour moteurs à réaction d'aérodynes*, 1952, French Patent FR1.008.660 (US Patent No. 2,692,480, "Supersonic internal circulation combustion chamber, in particular combustion chamber for aircraft jet engines," 1954).

[29] M. Roy, "Propulsion par statoreacteur a detonation," *Comptes Rendus Hebdomadaires des Séances de l'Académie des Sciences*, vol. 222, pp. 31–32, 1946, (Detonation Ramjet Propulsion).

[30] J. A. Nicholls, H. R. Wilkinson, and R. B. Morrison, "Intermittent detonation as a thrust-producing mechanism," *Jet Propulsion*, vol. 27, no. 5, pp. 534–541, 1957.

[31] R. A. Gross and A. K. Oppenheim, "Recent advances in gaseous detonation," *ARS Journal*, vol. 29, no. 3, pp. 173–179, 1959.

[32] R. A. Gross and W. Chinitz, "A study of supersonic combustion," *Journal of the Aerospace Sciences*, vol. 27, no. 7, pp. 517–524, 1960.

[33] W. H. Sargent and R. A. Gross, "A study of supersonic combustion," *ARS Journal*, vol. 30, no. 6, pp. 543–549, 1960.

[34] D. J. Vermeer, J. W. Meyer, and A. K. Oppenheim, "Auto-ignition of hydrocarbons behind reflected shock waves," *Combustion and Flame*, vol. 18, no. 3, pp. 327–336, 1972.

[35] T. E. Hutchins and M. Metghalchi, "Energy and exergy analyses of the pulse detonation engine," *Journal of Engineering for Gas Turbines and Power*, vol. 125, no. 4, pp. 1075–1080, 2002.

[36] J. A. C. Kentfield, "Thermodynamic cycle analysis of pulse detonation engine," *Journal of Propulsion and Power*, vol. 18, no. 1, pp. 68–76, 2002, doi: 10.2514/2.5899.

[37] Y. Wu, F. Ma, and V. Yang, "System performance and thermodynamic cycle analysis of airbreathing pulse-detonation engines," *Journal of Propulsion and Power*, vol. 19, no. 4, pp. 556–567, 2003.

[38] S. J. Jacobs, "The energy of detonation," U.S. Naval Ordnance Laboratory, White Oak, MD, NAVORD Report 4366, 1926.

[39] E. Wintenberger and J. E. Shepherd, "Model for the performance of airbreathing pulse-detonation engines," *Journal of Propulsion and Power*, vol. 22, no. 3, pp. 593–603, 2006.

[40] W. Fickett and W. C. Davis, *Detonation Theory and Experiment*. Mineola, New York: Dover, 2001.

[41] K. K. Kuo, *Principles of Combustion*, 2nd ed. New York: Wiley, 2005.

[42] J. H. S. Lee, *The Detonation Phenomenon*. New York: Cambridge, 2008.

[43] S. Gordon and B. J. McBride, "Computer program for calculation of complex chemical equilibrium compositions and applications, i: Analysis," NASA RP 1311, 1994.

[44] D. Goodwin, "Cantera: Object-oriented software for reacting flows," 2010. [Online]. Available: http://code.google.com/p/cantera

[45] Z. Y. Liu, "Overdriven detonation phenomenon and its application to ultra–high pressure generation," Ph.D. dissertation, Kumamoto University, 2001.

[46] S. Rao, "Effect of friction on the zel'dovich–von neumann–d" Master's thesis.

[47] T. Endo and T. Fujiwara, "Analytical estimation of performance parameters of an ideal pulse detonation engine," *Transactions of the Japan Society for Aeronautical and Space Sciences*, vol. 45, no. 150, pp. 249–254, 2003.

[48] T. Endo, T. Yatsufusa, S. Taki, A. Matsuo, K. Inaba, and J. Kasahara, "Homogeneous-dilution model of partially fueled simplified pulse detonation engines," *Journal of Propulsion and Power*, vol. 23, no. 5, pp. 1033–1041, 2007.

BIOGRAPHICAL STATEMENT

Ronnachai Vutthivithayarak was born in Bangkok, Thailand, in 1982 to Suthep and Phannee Vutthivithayarak. He received his B.Eng. in Aeronautical Engineering from the Royal Thai Air Force Academy, Thailand, in 2004, his M.Eng. in Systems Engineering from Shinawatra University, Thailand, in 2007. After working for three years in the Royal Thai Air Force, he got a scholarships for his Doctoral Degree. He joined the University of Texas at Arlington (UTA) for a Ph.D. in Aerospace Engineering. At UTA, Ronnachai's interests were mainly in aerodynamics, fluids, and energy conservation. He decided to work in Aerodynamics Research Center (ARC) in the area of pulse detonation engines for his dissertation with Prof. Frank Lu.